Prototypical oncogene family Myc defines unappreciated distinct lineage states of small cell lung cancer

Ayushi S. Patel[1,2], Seungyeul Yoo[3,4], Ranran Kong[1,2,5], Takashi Sato[1,2,6], Abhilasha Sinha[1,2], Sarah Karam[1], Li Bao[7], Maya Fridrikh[1,2], Katsura Emoto[8], German Nudelman[9], Charles A. Powell[1,2], Mary Beth Beasley[10], Jun Zhu[2,3,4], Hideo Watanabe[1,2,3,11*]

[1]Division of Pulmonary, Critical Care and Sleep Medicine, Department of Medicine, Icahn School of Medicine at Mount Sinai, New York, NY 10029, USA

[2]Tisch Cancer Institute, Icahn School of Medicine at Mount Sinai, New York, NY 10029, USA

[3]Department of Genetics and Genomic Sciences, Icahn School of Medicine at Mount Sinai, New York, NY 10029, USA

[4]Sema4, a Mount Sinai venture, Stamford, CT 06902, USA.

[5]Department of Thoracic Surgery, The Second Affiliated Hospital of Medical School, Xi'an Jiaotong University, Xi'an, Shaanxi, 710004, China

[6]Division of Pulmonary Medicine, Department of Medicine, Keio University School of Medicine, 35 Shinanomachi, Shinjuku, Tokyo 160-8582, Japan

[7] Ningxia People's Hospital, Yinchuan, Ningxia Province, China, 750001

[8]Department of Diagnostic Pathology, Keio University Hospital, 35 Shinanomachi, Shinjuku, Tokyo 160-8582, Japan

[9]Department of Neurology, Icahn School of Medicine at Mount Sinai, New York, NY 10029, USA

[10]Department of Pathology and Laboratory Medicine, Icahn School of Medicine at Mount Sinai, New York, NY 10029, USA

[11]Lead Contact

24 *Correspondence: hideo.watanabe@mssm.edu

25 *Summary: Historically well-known tumor promoting gene family plays a key role in cell identity*

26 *regulation in small cell lung cancer.*

Abstract

Comprehensive genomic analyses of small cell lung cancer (SCLC) have revealed frequent mutually exclusive genomic amplification of *MYC* family members. Hence, it has been long suggested that they are functionally equivalent; however, more recently, their expression has been associated with specific neuroendocrine markers and distinct histopathology. Here, we explored a novel role of L-Myc and c-Myc as lineage determining factors contributing to SCLC molecular subtypes and histology. Integrated transcriptomic and epigenomic analyses showed that L-Myc and c-Myc impart neuronal and non-neuroendocrine associated transcriptional programs, respectively, both associated with distinct SCLC lineage. Genetic replacement of c-Myc with L-Myc in c-Myc-SCLC induced a neuronal state but was insufficient to induce ASCL1 lineage. In contrast, c-Myc induced transition from ASCL1-SCLC to NeuroD1-SCLC characterized by distinct LCNEC-like histopathology. Collectively, we characterize a role of historically defined general oncogenes, c-Myc and L-Myc, for regulating lineage plasticity across molecular subtypes as well as histological subclasses.

42 **Introduction**

43 Small cell lung cancer (SCLC) represents about 15% of all lung cancers with a median
44 survival time of approximately 10 months and 5-year overall survival at 6% (*1*). SCLCs are
45 characterized by neuroendocrine differentiation, rapid growth, early metastatic spread and poor
46 prognosis (*2*). The standard of care has remained cytotoxic chemotherapy for decades, mainly
47 etoposide combined with a platinum agent (*3*) , which are only temporarily effective for the vast
48 majority of patients (*4*). Even with recent developments in immune checkpoint inhibitors,
49 activity against SCLCs when combined with chemotherapy has been marginal with a modest
50 improvement in the median survival (10.3 months vs. 12.3 months) for extensive stage SCLCs
51 treated with immunotherapy (*5*). These data reflect the urgent need for more effective
52 therapeutics for patients with SCLC. The lack of effective therapeutics for SCLC stands in stark
53 contrast to the breadth of targeted therapies for non-small cell lung cancer (NSCLC), particularly
54 lung adenocarcinoma (*6*). The progress in drug development for NSCLCs is largely attributable
55 to more comprehensive understanding of molecular subtypes and to identification of targetable
56 driver oncogenes (*7*). Therefore, better characterization of the molecular subtypes of SCLC
57 should aid future drug development and permit patient stratification for targeted therapies, a
58 strategy that has been remarkably effective for specific subsets of advanced lung
59 adenocarcinoma patients.

60 Characterization of SCLC subtypes was first noted by morphological differences over
61 three decades ago when human SCLC cell lines were implanted as xenografts and distinguished
62 as two primary subtypes: classic and variant SCLC (*8*, *9*). The classic subtype featured relatively
63 small cells with high nuclear:cytoplasm ratio, while the variant subtype exhibited relatively
64 larger cells and moderate amounts of cytoplasm. However, the World Health Organization

65 (WHO) classification, updated in 2015, histologically recognizes SCLC as a homogenous
66 disease with neuroendocrine features defined by small cells, scant cytoplasm, nuclear
67 morphology with fine granular chromatin, and lacking prominent nucleoli, reminiscent of the
68 features of the 'classic' SCLC. The originally described 'variant' subtype may represent
69 combined SCLC with LCNEC in the current classification (*10*).

70 More recent efforts to distinguish SCLC molecular subtypes include profiling gene
71 expression and genome-wide methylation in primary human tumors and patient derived
72 xenografts (PDX). These profiles revealed three clusters, with a dichotomy between achaete-
73 scute homologue 1 (ASCL1) and neurogenic differentiation factor 1 (NeuroD1) expression, in
74 addition to a cluster with low expression of both (*11*). The expression of ASCL1 and NeuroD1
75 has been implicated to confer SCLC heterogeneity by imparting distinct transcriptional profiles
76 (*12*). The third neuroendocrine-low cluster led to further classification into two subtypes
77 characterized by transcriptional driver YAP1 or POU class 2 homeobox 3 (POU2F3) (*13*, *14*).
78 SCLC cell line xenograft histology has been correlated with these contrasting factors, where
79 variant SCLC was positively correlated with a higher NeuroD1:ASCL1 ratio, and classic SCLC
80 was positively correlated with a higher ASCL1:NeuroD1 ratio in SCLC cell lines (*11*).

81 Observations on Myc family characteristics in SCLC genetically engineered mouse
82 models (GEMMs) have provided insight in their contribution to histopathological characteristics
83 (*15*, *16*). The SCLC GEMM with conditional loss of *Rb1* and *Trp53* mouse (RP), harbored
84 stochastic *MYCL* amplifications or overexpression associated with classic SCLC histopathology
85 (*17*). On the contrary, consistent with the original report on the variant subtype to harbor
86 frequent *MYC* amplification (*9*), a more recent study showed that additional c-Myc

87 overexpression, in the RP SCLC GEMM, drives the progression of murine SCLC with variant
88 histopathology and reduced neuroendocrine gene expression including ASCL1 but higher
89 NeuroD1 expression (*18*). Yet, the molecular mechanisms underlying the distinction between L-
90 Myc and c-Myc driven subsets of SCLC remain unexplored.

91 c-Myc (*MYC*) and L-Myc (*MYCL*) belong to the MYC family of basic helix-loop-helix
92 (bHLH) transcription factors. The paralogs contain functionally relevant highly conserved amino
93 acid sequences and are structurally homologous (*19*, *20*). c-Myc is a well-characterized
94 oncogene; L-Myc, although understudied, is implicated to have a similar oncogenic role.
95 Amplification of Myc family members is mutually exclusive and overall accounts for ~20% of
96 SCLC and overexpression for ~50% of SCLC in primary human tumors (*21*). In contrast to the
97 fact that *MYC* is commonly amplified across all three major lung cancer subtypes; lung
98 adenocarcinomas, squamous cell lung carcinomas and SCLC (*21–23*), *MYCL* and *MYCN* are
99 uniquely amplified in SCLC, in a manner suggestive of their role as lineage-amplified genes.

100 In this study, we explored a novel role of c-Myc and L-Myc as lineage specific factors to
101 associate SCLC molecular subtypes with histological classes. We investigated the potential of L-
102 Myc and c-Myc to regulate lineage state and identified transcriptional programs unique to each
103 Myc family member, wherein L-Myc regulates neuronal developmental pathways and c-Myc
104 regulates epithelial-to-mesenchymal transition and Notch signaling, biological pathways that are
105 associated with distinct molecular subsets. We showed c-Myc expression is required to maintain
106 lineage state marker NeuroD1 in NeuroD1-positive SCLC. In addition, c-Myc is and is
107 incompatible with ASCL1-positive SCLC that ultimately leads to trans-differentiation to

108 NeuroD1-SCLC, consistent with previous findings (*24*). Furthermore, this trans-differentiation is
109 characterized by variant histopathology mediated by a transcriptional repressor, Rest.

110

111 **Results**

112 *SCLC network reveals unique and distinct sub-networks for c-Myc and L-Myc*

113 To understand biological processes that may be unique to c-Myc and L-Myc in SCLC, we
114 sought to investigate potential causal regulations among genes. To this end, we first built a
115 molecular causal network using primary SCLC datasets and then focused on networks that
116 involve c-Myc and L-Myc. Combining two independent primary SCLC transcriptomic datasets
117 (*21*, *25*), we built a Bayesian network using RIMBANET, a software package we previously
118 developed (see Methods). The Bayesian network comprised 8,451 unique genes (nodes) and
119 9,301 regulations (edges) among these genes. The regulations inferred in this Bayesian network
120 provide insights into biological functions associated with molecular features such as pathways or
121 gene signatures (*26*, *27*). This enables us to discern transcriptional sub-networks associated with
122 c-Myc and L-Myc that may reflect their unique biological roles. We first aimed to generate a
123 signature associated with each factor and then project the signature to the SCLC Bayesian
124 network to identify specific subnetworks (Figure 1A). To generate these signatures, we sought to
125 select an independent dataset. Hence, we examined copy number alteration and expression for
126 each Myc family member in 49 SCLC cell lines from Cancer Cell Line Encyclopedia (CCLE)
127 and classified them into four groups representing each Myc family member and low Myc (Figure
128 S1A). Then, we selected cell lines that belong to *MYC* and *MYCL* groups and examined mRNA
129 expression *MYC* and *MYCL* to select cell lines for c-Myc with high expression of *MYC* and low
130 expression of *MYCL* and vice versa (Figure S1B). We identified 457 differentially expressed

131 genes (t-test p-value < 0.01 and fold change > 1.5), 147 and 310 genes overexpressed in *MYC*
132 and *MYCL* SCLC cell lines respectively and defined them as their introductory gene signatures
133 (Figure S1C and Table S1).

134 To explore the sub-networks associated with L-Myc, we projected the genes upregulated in
135 the L-Myc expressing subset onto the network and collected all nodes within two layers from
136 them (see Methods). We identified one large closed sub-network (L1, Figure 1B) that comprises
137 959 gene nodes that included 120 of 310 genes from the L-Myc signature. To identify master
138 regulators of the L-Myc subnetwork, we performed Key Driver Analysis (see Methods) that
139 revealed 13 statistically significant genes (Table S2). Examining protein expression of Smad2, a
140 node in the L-Myc sub-network, revealed higher expression in L-Myc-classified cell lines
141 compared to c-Myc-classified cell lines (Figure S1D). Gene ontology analysis of this L-Myc
142 subnetwork revealed enrichments of two biological processes: cell cycle progression and
143 neuronal development (Figure 1C). These processes have been previously implicated as core
144 descriptors of classic SCLC (*2*). On the other hand, when we projected the c-Myc signature onto
145 the network, the c-Myc network was organized into three unique sub-networks, c1, c2 and c3,
146 consists of 25, 95, and 29 gene nodes, respectively (Figure 1D). Key Driver Analysis of all three
147 sub-networks revealed 15 statistically significant regulators (Table S3). Sub-network c1 was
148 enriched for canonical c-Myc functions in transcriptional, translational and metabolic regulation
149 (Figure 1E) (*20*). c-Myc sub-network c2 was enriched for pathways in epithelial-to-mesenchymal
150 transition (Figure 1E); that has been shown to be relevant in the neuroendocrine-low subtype
151 (*28*). Finally, c-Myc sub-network c3 was enriched for Notch signaling pathway (Figure 1E),
152 which has been implicated to mediate a transition from neuroendocrine to non-neuroendocrine
153 fate of tumor cells in a murine SCLC model (*29*). These functional pathways enriched in

154 subnetworks c2 and c3 describe a relationship between c-Myc and lineage state determination
155 pathways in SCLC.

156 Together, these findings suggest that c-Myc and L-Myc are associated with different
157 molecular mechanisms that have been implicated in SCLC biology. Specifically, it implicates c-
158 Myc is associated with neuroendocrine-low differentiation state in addition to its canonical
159 oncogenic functions in SCLC, and by contrast, L-Myc is associated with classic neuroendocrine
160 state of SCLC.

161

162 *c-Myc and L-Myc driven SCLCs exhibit distinct chromatin states to exert differential*
163 *transcriptional programs*

164 Next, we sought to determine whether the distinct c-Myc and L-Myc networks are
165 associated with their distinct cistromes. To examine the role of each Myc family member, we
166 selected representative cell lines for c-Myc (NCI-H82, NCI-H524, NCI-H2171 and NCI-H2081)
167 and L-Myc (CORL-88, NCI-H1963 and NCI-H209) based on the classification described in
168 (Figure S1A) and confirmed protein expression for these transcription factors (Figure 2A). Of
169 note, NCI-H1963 expressed MYCL-RLF fused protein as well as the wild-type protein. The
170 fused protein which lacks the first 27 amino acids of L-Myc and is fused to 79 amino acids of
171 RLF protein has been previously shown to be functional in SCLCs (*30*).

172 In order to define open regulatory elements potentially regulated by c-Myc and L-Myc,
173 we first performed the assay for transposase-accessible chromatin-sequencing (ATAC-seq) on
174 three representative cell lines for each Myc (selected from Figure 2A) and identified accessible
175 chromatin regions, then we filtered these regions with motif matrices for Myc binding (E-box)
176 referring to as Myc accessible regions hereafter (Figure 2B, See Methods). Of note, inferred Myc

177 accessible regions reasonably recapitulated c-Myc binding sites previously determined by c-Myc
178 chromatin-immunoprecipitation in NCI-H2171 cells (*31*) (Figures S2A and S2B). This approach
179 eliminates confounding factors from antibody-dependent sensitivity and specificity that are
180 intrinsic to ChIP based assays to compare cistromes of two distinct proteins.

181 Principal component analysis (PCA) of E-Box containing peaks in all six cell lines, separated
182 these cell lines according to Myc status (Figure 2C). Additionally, a correlation matrix of
183 pairwise Pearson correlation coefficient of Myc accessibility signal captured distinct clusters for
184 the c-Myc and L-Myc classified cell lines (Figure S2C). Examining genome-wide Myc
185 accessible regions in each individual cell line, we observed a fraction of peaks that overlapped
186 between c-Myc classified and L-Myc classified cells (cluster 1; Figure 2D), suggestive of
187 common functional binding that the Myc family members share. We also found distinct groups
188 of peaks with higher signal intensity unique to L-Myc classified cells (cluster 2; Figure 2D) and
189 in c-Myc classified cell lines (cluster 3; Figure 2D), suggesting distinctive DNA binding profiles
190 for L-Myc and c-Myc. We observed preferential accessibility at distinct genetic loci in L-Myc
191 cell lines when compared to c-Myc cell lines (Figure 2E). This included augmented accessibility
192 in L-Myc cell lines at lung and neuron development factor *FOXA2* (*32*, *33*) (Figure 2E) and
193 *POU3F2* (Brn2), a neuronal lineage factor of lung squamous cancer (Figure S2D) (*34*); while in
194 c-Myc cell lines at cell surface adhesion factor *ITGA4* (Figure 2E) and neuronal repressor, *REST*
195 (Figure S2E). Consistent with the epigenetic results, we found protein expression of Brn2 was
196 significantly higher in L-Myc-classified cell lines, and Rest expression was highest in two c-
197 Myc-classified cell lines with highest Myc accessibility at its locus while there was no
198 statistically significant difference between c-Myc and L-Myc classified cell lines (Figure S2F).
199 Of note, the chromatin landscape of NCI-H82 appeared to be intermediate to the L-Myc and c-

200 Myc profiles. Together, these findings reveal the commonality and distinction between c-Myc
201 and L-Myc binding profiles.

202 To gain insights into the unique biological processes c-Myc and L-Myc may impart, we
203 analyzed differentially enriched Myc accessible sites comparing c-Myc cell lines and L-Myc cell
204 lines. We identified 2,808 differentially accessible regions; 1,235 peaks enriched in L-Myc
205 classified cell lines and 1,573 peaks enriched in c-Myc classified cell lines (Figure 2F). Next, we
206 performed GREAT (Genomic Regions Enrichment of Annotations) analysis (*35*) on the
207 differentially accessible peaks. Unique L-Myc accessible sites were enriched for neuronal
208 pathways such as glial cell proliferation, development of the neural plate, neural fold and future
209 midbrain (Figure 2G). By contrast, unique c-Myc accessible sites were enriched for pathways
210 involved in Notch signaling (Figure 2H). While specific Notch signaling activity in *MYC*-
211 amplified SCLCs has not been previously noted, there have been previous reports showing Rest
212 as a target of the Notch signaling pathway to suppress the expression of neuronal genes (*21*, *24*,
213 *29*). These findings are consistent with the observations from the Bayesian network analysis,
214 providing additional evidence to suggest distinct transcriptional programs in c-Myc and L-Myc
215 driven SCLCs.

216 Next, to explore the relationship between c-Myc and L-Myc transcriptomic and epigenomic
217 signatures, we examined average Myc accessibility signal at L-Myc and c-Myc sub-network
218 genes in c-Myc- and L-Myc-classified cell lines, respectively. This analysis revealed L-Myc
219 subnetwork genes were preferentially accessible in L-Myc-classified cell lines while c-Myc
220 subnetwork genes were preferentially accessible in c-Myc lines when compared to all other
221 genes (Figures S3A and S3B). Gene set enrichment analysis (GSEA) of Myc accessible regions
222 revealed c-Myc specific accessible regions were significantly enriched for the introductory c-

223 Myc transcriptomic signature (defined in Figure S1C) while L-Myc specific accessible regions
224 were significantly enriched for the introductory L-Myc transcriptomic signature (Figure S3C),
225 confirming the consistency between two datasets. Altogether, these independent datasets reveal
226 concordant L-Myc and c-Myc signatures to distinguish the two factors.
227
228 *c-Myc and L-Myc expression is associated with distinct lineage state markers*
229 A recent review synthesized SCLC profiling studies to identify four molecular subtypes,
230 where two of these subtypes are classified as neuroendocrine SCLC that are driven by either
231 ASCL1 or NeuroD1, and the other two are classified as non-neuroendocrine driven by YAP1 or
232 POU2F3 (*6*). Given our findings from the Bayesian network and Myc accessibility profiling that
233 c-Myc and L-Myc regulate transcriptional programs associated with distinct lineage determining
234 programs, we sought to investigate the relationship between Myc family members and the
235 proposed SCLC master regulator classifiers.
236 Myc accessibility profile at the individual locus level of our c-Myc and L-Myc classified cell
237 lines for these four factors revealed augmented accessibility in the c-Myc classified cell lines at
238 the *NEUROD1* locus in contrast to L-Myc classified cell lines that had augmented accessibility at
239 the *ASCL1* locus (Figures S4A and S4B). We observed no differential or preferential
240 accessibility signal in either c-Myc classified and L-Myc classified cell lines at *POU2F3* and
241 *YAP1* loci likely reflecting that these cell lines do not represent these subtypes (Figures S4C and
242 S4D). Protein expression of these lineage state markers showed that our L-Myc classified cell
243 lines had exclusive expression of ASCL1, while the c-Myc classified cell lines exclusively
244 expressed NeuroD1, consistent with the chromatin profile. (Figure S4E).

245 To understand how c-Myc and L-Myc expression correlated with the four molecular subtypes
246 in CCLE cell lines, we examined the expression of c-Myc and L-Myc in each of the molecular
247 subtypes as classified in (*6*). We observed that the non-neuroendocrine, POU2F3 and YAP1, as
248 well as NeuroD1 subtypes had higher expression of c-Myc (Figure S4F). On the other hand, L-
249 Myc expression was enriched in the neuroendocrine high ASCL1 subtype (Figure S4G).

250 We further sought to reproduce the classification with data from primary tumors (*21*) and
251 CCLE cell lines with additional data from 77 primary tumors (*25*) (Figure 3A, Table S4). Of
252 note, while our unsupervised clustering was in general agreement with the published
253 classification (*6*), the ASCL1 subtype cluster revealed heterogeneity particularly of primary
254 tumors with the dual expression of ASCL1 and other lineage factors that may indicate lineage
255 transition or intra-tumor heterogeneity (Figure 3A). In this classification, we found that L-Myc
256 expression was higher in samples classified as ASCL1 or NeuroD1 subtype when compared to
257 the non-neuroendocrine subtype, thus indicating unique expression of L-Myc in neuroendocrine
258 SCLC (Figure 3B). On the other hand, the expression of c-Myc was higher in tumors and cell
259 lines clustered in the NeuroD1 subtype and non-neuroendocrine low, POU2F3 and YAP1, as
260 compared to those classified as ASCL1 (Figure 3C), suggesting a negative relationship between
261 ASCL1 and c-Myc. Indeed, we found the expression of c-Myc is anti-correlated with ASCL1 (r
262 = -0.53) across the combined primary tumor and cell line datasets (Figure 3D). Together, these
263 data imply the dichotomy of c-Myc expression and L-Myc expression in SCLC lineages.

264

265 *L-Myc induces a neuronal state but fails to transition to ASCL1 expressing SCLC*

266 Given that L-Myc expression and c-Myc expression are enriched in distinct subtype(s),
267 and they regulate programs associated with its respective subtype, we hypothesized that part of

268 the role Myc family members play is to serve as a lineage factor. To test the potential of L-Myc
269 to establish the neuroendocrine lineage, we modified two c-Myc expressing NeuroD1 classified
270 cell line NCI-H82 and NCI-H524 by exogenous overexpression of L-Myc and CRISPR-Cas9
271 mediated deletion of c-Myc (Figure 4A). We found c-Myc expressing cell line, NCI-H82 and
272 NCI-H524 was able to tolerate the over-expression of L-Myc (Figures 4B, S5A and S5B). Cells
273 engineered to express both L-Myc and c-Myc exhibited comparable proliferation rates compared
274 to parental cells expressing only c-Myc (Figures 4C and S5C). We further demonstrated that
275 replacement of c-Myc with the expression of L-Myc allowed the cells to retain proliferative
276 potential in the absence of c-Myc in NCI-H82 and NCI-H524 (Figures 4C and S5C). This
277 indicates redundant roles among the two Myc family members in regards to maintaining cell
278 viability.

279 To inquire their contribution to lineage determination, we evaluated the expression of
280 lineage state markers on day 5. Addition of L-Myc neither induced expression of
281 neuroendocrine-marker ASCL1 nor altered the expression of NeuroD1 (Figures 4B and S5B). By
282 contrast, the replacement of c-Myc with L-Myc led to the downregulation of NeuroD1 (Figures
283 4B and S5B). The lack of expression of alternate neuroendocrine lineage marker ATOH1,
284 neuroendocrine-low lineage state markers YAP1 and POU2F3 in these ASCL1- and NeuroD1-
285 negative cells in both NCI-H82 and NCI-H524, indicates a unique lineage negative state for
286 these cells (Figures S5D and S5E).

287 Without L-Myc replacement, consistent with previous findings (*36*), c-Myc was essential
288 for survival in NCI-H82 (Figure 4C), thus precluding us from evaluating converted lineage state.
289 However, during the short window of survival, c-Myc ablation led to significant downregulation

290 of NeuroD1 suggesting a role of c-Myc on maintaining expression of lineage state marker
291 (Figure 4D and S5F).

292 Even with the loss in lineage marker expression, we observed no significant
293 morphological changes *in vitro* (Figure S5G). However, morphological characteristics in
294 suspension cells can be but are not always reflective of a neuroendocrine or non-neuroendocrine
295 state. Previous literature showed that deletion of *Mycl* (L-Myc) in the RP GEMM resulted in
296 tumors with mixed and NSCLC morphology (*16*) in contrast to the c-Myc expressing SCLC with
297 'variant' morphology (*9*, *18*). Therefore, to investigate L-Myc's contribution to SCLC histology,
298 we implanted genetically engineered NCI-H82 cells into immunodeficient mice. Histological
299 analysis of NCI-H82 expressing L-Myc and NCI-H82 L-Myc ablated with c-Myc xenografts
300 revealed morphology similar to the control NCI-H82-LacZ/sgNT cells with polygonal cells,
301 large nucleoli and moderate amounts of cytoplasm representative of 'variant' SCLC consistent
302 with previous reports (*9*) (Figure S5H). The insufficiency of L-Myc to induce histological trans-
303 differentiation may partially explain the low frequency of transition from variant to classic SCLC
304 (*29*).

305 To investigate the state of these lineage-marker negative cells, we performed
306 transcriptomic profiling. Gene ontology analysis of 235 significantly upregulated genes by L-
307 Myc in the presence of c-Myc in NCI-H82 revealed enrichment for neurogenesis and neuronal
308 associated pathways (Figures S6A and S6B), suggesting that L-Myc imparts neuronal pathways
309 while not fully inducing ASCL1-lineage state. Ablation of c-Myc further upregulated 170 genes
310 compared to the previous condition, which are enriched for neuronal structure, suggesting the
311 cells are further committed to a neuronal state (Figure S6C and S6D). A direct comparison of the
312 control NCI-H82 cells with lineage negative-NCI-H82 cells revealed 713 significantly

313 upregulated genes enriched for neuronal associated pathways and 500 downregulated genes
314 enriched for canonical Myc function (Figures 4E, 4F and S6E). Collectively, indicating the
315 significance of L-Myc in inducing a more neural state. Next, to investigate which state these
316 lineage-marker negative cells most closely resemble, we compared the transcriptomic profile of
317 these genetically engineered cells to cell lines classified as ASCL1, NEUROD1, YAP1 and
318 POU2F3. PCA of these cell lines revealed with the replacement of c-Myc with L-Myc in NCI-
319 H82 cells clustered away from NEUROD1, YAP1 and POU2F3 cells and shifted towards
320 ASCL1-classified cell lines (Figure S6F). To more clearly see the shift, we compared the state of
321 these cells only to ASCL1- and NEUROD1- SCLC that revealed replacement of c-Myc with L-
322 Myc in NCI-H82 cells transitioned the cells closer to ASCL1 (Figure 4G). Together, these data
323 suggest that replacement of c-Myc with L-Myc although, induces a more neural state but does
324 not fully transdifferentiates to ASCL1-positive state and remains to be negative for lineage
325 markers used in the current consensus molecular classification (*6*).

326 To investigate how L-Myc rewires the Myc accessible landscape, we profiled Myc-
327 accessible regions of 3 NCI-H82 control cells (LacZ, LacZ/sgNT1, and LacZ/sgNT2), and 3
328 NCI-H82 with c-Myc replaced by L-Myc (L-Myc/sg*MYC*1, L-Myc/sg*MYC*2 and L-
329 Myc/sg*MYC*3). Analysis of genome-wide Myc accessibility in control cells and replacement
330 cells identified a common cluster of Myc accessible regions, indicating an aspect of functional
331 redundancy between c-Myc and L-Myc (cluster 1; Figure 4H). Additionally, we identified
332 unique clusters gained and lost with L-Myc over-expression and c-Myc deletion (clusters 2 and
333 3; Figure 4H). To investigate what these unique clusters represent, we identified 1,165 regions
334 uniquely enriched in replaced NCI-H82 cells compared to the controls (Figure 4I). Integrative
335 ontology analysis of these regions with the transcriptomic profile (from Figure 4E) revealed

336 enrichment for neuronal associated pathways, suggesting direct activation of these genes (Figure
337 4J, top panel). On the other hand, Myc accessible regions lost with this genetic engineering were
338 enriched for functions to maintain high metabolic state that have been reported to be regulated by
339 Myc (Figure 4J, bottom panel). These data suggest that L-Myc has the potential to upregulate
340 neuronal lineage associated pathways, suggestive of its lineage determining function in SCLC.
341
342 *Aurora Kinase A Inhibition sensitivity is altered with change in Myc status*
343 Previous findings suggest that *MYC* (c-Myc)-driven SCLC is more responsive to Aurora
344 kinase A inhibition (*18*, *37*). We confirmed previous findings that *MYC*-amplified cell lines
345 exhibit increased sensitivity and *MYCL*-amplified cell lines are resistant to alisertib (Figure
346 S7A). Alisertib treatment of the NCI-H82 cells expressing both c-Myc and L-Myc revealed no
347 changes in sensitivity to the drug nor did changes in expression of the variant state marker.
348 However, the cells that replaced c-Myc with L-Myc became resistance to aurora kinase
349 inhibition (Figure S7B). On the other hand, overexpression of c-Myc increased sensitivity at
350 lower concentrations of the drug (Figure S7C). This suggests either alisertib sensitivity is
351 attributable to c-Myc driven lineage state of the cells, or difference in molecular interaction of
352 Aurora kinase A with each Myc protein.
353
354 *c-Myc causes loss of classic neuroendocrine SCLC features*
355 The dependency of lineage state marker NeuroD1 on c-Myc led us to hypothesize that c-
356 Myc exerts a role in addition to its oncogenic role to regulate and establish a variant
357 differentiation state. To this end, we genetically engineered a neuroendocrine-high L-Myc
358 expressing NCI-H1963 and NCI-H187 with exogenous overexpression of c-Myc (Figures 5A

359 and 5B). Of note, exogenous expression of c-Myc led to downregulation of L-Myc in NCI-
360 H1963 and NCI-H187 (Figures 5A, 5B, S8A and S8B).

361 When c-Myc expression is introduced in NCI-H1963 or NCI-H187, we observed an
362 initial phase of growth suppression (Figures 5C and 5D). This observation stands in contrast to
363 the established role of c-Myc to promote cell cycle and cell proliferation (*38*). The growth
364 suppression is unlikely to be due to oncogene induced senescence as these cells stained negative
365 for beta-galactosidase (Figure S8C) and are deficient for Rb1 and p53. We investigated the cell
366 cycle dynamics in their growth suppressive phase and found that initial c-Myc expression (day 2)
367 modestly increased the proportion of cells in S and G2/M phase but did not significantly alter the
368 distribution of cells or induce cell cycle arrest to explain slower cell growth (Figure S8D).
369 Alternatively, we investigated the proportion of Annexin-V positive cells on day 2 and found c-
370 Myc overexpression increased the proportion of necrotic and apoptotic cells as compared to
371 control cells (Figures 5E and S8E) in NCI-H1963.

372 We hypothesized that cell death was a consequence of incompatibility of the
373 neuroendocrine differentiation state with c-Myc expression and that the persisting cells
374 eventually grown out were cells that tolerated the expression of c-Myc, potentially by trans-
375 differentiating to a state compatible with c-Myc expression (Figure 5C and 5D). Note that we
376 define trans-differentiation as change in cancer lineage state by the expression of lineage markers
377 and histological features, not a conversion to a different lineage hierarchy. Therefore, we
378 investigated the expression of lineage state markers and found that the overexpression of c-Myc
379 downregulated ASCL1 and upregulated NeuroD1 in NCI-H1963 and NCI-H187 cells (Figure 5A
380 and 5B), indicating the trans-differentiation to NeuroD1-subtype of SCLC and that c-Myc exerts

381 a role in dictating a distinct NeuroD1-positive neuroendocrine differentiation state. We observed
382 no significant morphological changes in these cells *in vitro* (Figure S8F).

383 To investigate if the trans-differentiation between molecular subtypes was accompanied
384 by histological switch *in vivo*, we injected NCI-H1963 cells genetically engineered with stable c-
385 MYC expression. Tumor growth dynamics recapitulated the slower growth of c-Myc
386 overexpressed NCI-H1963 observed *in vitro* (Figure S9A). This was associated with comparable
387 levels of proliferation measured by Ki67 and increased levels of apoptosis measured by cleaved
388 Caspase-3 (Figure S9B). We observed that NCI-H1963 overexpressed with LacZ (control cells)
389 had oval and elongated nuclei with a high nuclear:cytoplasm ratio, smooth granular chromatin
390 and no nucleoli consistent with classic SCLC histology (Figure 5F and S9C), similar to the
391 histology that would be typically diagnosed with SCLC in primary human tumors (Figure 5G).
392 Histological analysis of xenografts of NCI-H1963 overexpressed with c-Myc showed presence
393 of nucleoli and polygonal shaped larger cells, reminiscent of variant SCLC histology as defined
394 by (*9*) (Figure 5F, Figure S9C). The histopathology observed here, according to the current
395 WHO classification, would likely be recognized as either purely LCNEC or "combined SCLC"
396 that includes a component of large-cell neuroendocrine carcinomas (LCNEC), potentially
397 reflective of the discrepancies between clinical practice and experimental findings (Figure 5G)
398 (*10*, *39*). Together, these results suggest that c-Myc expression drives the transition from
399 ASCL1-positive state characterized by classic SCLC histology to NeuroD1-positive state SCLC
400 characterized by 'variant' SCLC or LCNEC histology.

401 To examine the relevance of c-Myc expression in LCNEC, we compared distribution of
402 its mRNA expression levels in tumors diagnosed as LCNEC (*40*) and those diagnosed as SCLC
403 (*21*). After batch correction, we found a greater proportion of LCNEC tumors express c-Myc at

404 a level comparable to c-Myc expressing SCLC (Figure S9D). These data suggest c-Myc
405 expression is likely as relevant in human LCNEC as in SCLC and are consistent with the
406 evidence where c-Myc overexpression can induce histological characteristics reminiscent of
407 LCNEC in our model, while it does not necessarily indicate that LCNEC histology is defined by
408 the expression of c-Myc.

409

410 *c-Myc mediates trans-differentiation through REST*

411 We sought to investigate the mechanism through which c-Myc mediates trans-
412 differentiation to the ASCL1-negative/NeuroD1-positive state. To this end, we profiled the
413 accessible chromatin profile of trans-differentiated NCI-H1963. Filtering the regions to reflect
414 regions with Myc (E-box) motif matrices reflected a common pattern (clusters 1 to 4). c-Myc
415 overexpression resulted in the gain of additional regulatory regions (cluster 5) and a decrease in
416 accessibility at a fraction of sites in cluster 6 (Figure 6A), revealing an alteration of the Myc (E-
417 box) cistrome and further suggesting non-redundancy of this family of transcription factors.
418 Next, we sought to investigate how the re-wiring of these regulatory regions compared to c-Myc
419 and L-Myc expressing SCLC. PCA of Myc accessibility in these genetically engineered cells and
420 c-Myc and L-Myc classified cell lines revealed NCI-H1963 expressing c-Myc clustered closer to
421 c-Myc classified cell lines along Principal Component (PC) #1, mapping NCI-H1963
422 transitioning from L-Myc cistrome towards a c-Myc cistrome (Figure 6B). These data re-iterate
423 c-Myc mediated alteration in regulatory regions that dictate cellular identity.

424 To identify the transcriptional programs associated with the changes in regulatory regions
425 of the Myc cistrome, we performed RNA-seq on trans-differentiated NCI-H1963. We identified
426 775 differentially expressed genes (375 upregulated genes downregulated and 400

427 downregulated genes) (Figure 6C). Gene ontology analysis for upregulated genes revealed an
428 enrichment for epithelium development in addition to canonical c-Myc functions including
429 regulation of cell proliferation and regulatory region nucleic acid binding (Figure 6D, left panel)
430 while gene ontology analysis for downregulated of genes revealed an enrichment for neuronal
431 associated genes (Figure 6D, right panel). These findings suggest c-Myc expression in ASCL1
432 expressing SCLC induces a transition to a more epithelial state and are consistent with the loss in
433 neuroendocrine lineage state marker (Figure 5A), but did not reveal further specific mechanistic
434 insights.

435 Previous works have shown the negative regulation of ASCL1 by Notch signaling during
436 lung development (*41*) and activation of Notch signaling in SCLC suppresses ASCL1 expression
437 (*21*, *42*, *43*). Additionally, our SCLC transcriptional network analysis and Myc accessibility data
438 revealed Notch pathway activation preferentially in c-Myc expressing tumors and cell lines
439 (Figures 1E and 3C). Although, we did not observe an enrichment for an active Notch signaling
440 signature amongst the upregulated genes, when we investigated the expression of known Notch
441 signaling pathway targets in trans-differentiated NCI-H1963 (*24*), we identified Notch-target
442 RE-1 Silencing transcription factor (REST) was induced upon c-Myc expression (Figure 7A and
443 7B). Prior works have shown that Rest acts as a neuronal differentiation repressor (*44*) and REST
444 inhibition removes neural reprogramming block that allows for the conversion to neuronal fate in
445 human adult lung and dermal fibroblasts (*45*). Therefore, we overexpressed Rest expression in
446 NCI-H1963 and inquired the status of ASCL1, and found that Rest in this context can also
447 mediate the suppression of ASCL1 (Figure 7C).

448 To further investigate if Rest is required for c-Myc mediated suppression of ASCL1 in
449 SCLC, we deleted REST mediated by CRISPR-Cas9 prior to c-Myc overexpression in NCI-

450 H1963 cells. Suppression of Rest reversed c-Myc overexpression-induced decrease in the level
451 of ASCL1 (Figure 7D). Simultaneous pharmacological inhibition of Rest (*46*) and c-Myc over-
452 expression on NCI-H1963 cells recapitulated these findings (Figure 7E). Further, ChIP-qPCR for
453 Rest in c-Myc overexpressed NCI-H1963 indicated that Rest associates more significantly with
454 the *ASCL1* and *MYCL* loci compared to control LacZ overexpressed NCI-H1963, suggesting
455 Rest directly modulates the expression of these neuroendocrine markers (Figure 7F).

456 In murine SCLC cells, gain of Rest expression has been associated with active Notch
457 signaling that downregulate the expression of Ascl1 (*29*). Therefore, we sought to investigate the
458 c-Myc–Notch–Rest axis in mediating trans-differentiation. Pharmacological inhibition of Notch
459 using a γ-secretase inhibitor (GSI), DBZ (*47*) and DAPT in combination with c-Myc expression
460 in NCI-H1963 cells reduced the level of Hes1, confirming a suppression of the pathway, but did
461 not alter expression of Rest and ASCL1 (Figures 7G and 7H). Therefore, we investigate how c-
462 Myc activates the expression of Rest, we performed c-Myc ChIP-qPCR on c-Myc overexpressed
463 NCI-H1963 cells and found c-Myc binding is more enriched at the *REST* locus but not at the
464 *ASCL1* locus compared to NCI-H1963 LacZ control cells, suggesting c-Myc directly, at least
465 partially, modulates the expression of Rest (Figure 7I). Together, these data suggest a novel
466 Notch-independent, c-Myc mediated activation of Rest and Rest mediated-suppression of
467 ASCL1.

468

469 **Discussion**

470 In this study, we showed a novel functional distinction between c-Myc and L-Myc in SCLC.
471 Moreover, our data from functional replacement of c-Myc with L-Myc in c-Myc-SCLC suggest
472 that c-Myc is responsible for the maintenance of NeuroD1 expression and further replacement

473 with L-Myc leads to transition into a neuronal state more similar to ASCL1-SCLC; however, it
474 does not shift into full ASCL1-SCLC state but instead to neuronal lineage-negative state. On the
475 other hand, c-Myc overexpression in ASCL1-SCLC with classic SCLC histology resulted in
476 trans-differentiation to NeuroD1-SCLC accompanied by LCNEC-like/variant SCLC histology
477 partially mediated through the direct upregulation of Rest (Figure 7J).

478 We describe c-Myc is associated not only with canonical roles including transcriptional and
479 translational regulation, but also with lineage associated pathways such as Notch signaling and
480 epithelial-mesenchymal transitions. Our findings are supported by a previous report that
481 described active Notch signaling negatively regulating neuroendocrine lineage by suppressing
482 the expression of *ASCL1* (*29*) as well as a study that showed mesenchymal-like features in
483 neuroendocrine-low sub-type of SCLC (*28*). On the other hand, we found L-Myc is associated
484 with neuronal pathways implicating their relevancy in determining the classic neuroendocrine
485 state of SCLC. These findings are consistent with previous observation showing a correlation of
486 expression between L-Myc and neuronal proteins (*28*, *48*). Taken together, contrary to the notion
487 that Myc family members, c-Myc in particular, exclusively act as oncogenes and general
488 amplifiers of expression and metabolism, our data suggest that they additionally exert lineage
489 defining transcriptional programs (*24*). We propose that the Myc family members regulate a
490 defined set of transcriptional programs that are essential in SCLC lineage subtype determination.
491 Of note, these biological pathways have been implicated for lineage maintenance and
492 determination in distinct subtypes of SCLC and correlated to different Myc family members
493 (*28*); here we show that Myc family members indeed regulate these SCLC lineage associated
494 pathways.

495 We found L-Myc failed to induce the expression of a neuroendocrine lineage state marker
496 ASCL1, suggesting its inability to fully control trans-differentiation from neuroendocrine-
497 low/variant state to neuroendocrine high/classic state. However, based on previous work
498 suggesting requirement of L-Myc to drive tumors of neuroendocrine origin in SCLC GEMM
499 (*16*) and our findings that revealed L-Myc regulating and inducing neuronal development
500 pathways, L-Myc likely plays roles in lineage state maintenance and/or is more compatible with
501 the neuroendocrine lineage.

502 Here, we report the functional importance of c-Myc in regulating cellular states (*18*, *24*). We
503 also report a previously undescribed function for c-Myc in lineage maintenance in NeuroD1-
504 positive SCLC. c-Myc expression was incompatible with ASCL1-positive SCLC and induces
505 trans-differentiation to NeuroD1-positive state revealing the role for c-Myc in regulating lineage
506 plasticity (*24*). We show that this trans-differentiation between molecular subtypes of SCLC is
507 accompanied by alterations in the transition of histopathology in SCLC from classic SCLC
508 features to variant histopathology. These data reflect that the variant histopathology, that would
509 typically be classified as "combined" SCLC or LCNEC per the current guidelines of WHO, can
510 indeed be derived from SCLC. This itself has significant clinical implication. This phenotype is
511 reflective of biology distinct from classic SCLC consistent with prior reports (*14*, *18*, *37*, *49*) and
512 therefore, warrant distinct therapeutic strategies.

513 We identified that the trans-differentiation is mediated independent of Notch signaling but
514 through the direct activation of a Notch signaling target, Rest, a transcriptional repressor. These
515 findings may be clinically important when evaluating the rationale for targeting SCLC by
516 activating Notch signaling with drugs including LSD1 and KDM5A (*42*, *43*). Our data suggests

517 that downstream actors of Notch signaling induces c-Myc mediated trans-differentiation. This
518 may not be a favorable outcome since the variant subtype has been reported to be more frequent
519 in tumors after initial response to chemotherapy (*9*, *18*). We found that the altered differentiation
520 state with the gain of L-Myc and loss of c-Myc cells conferred resistance to Aurora Kinase A
521 inhibition and in contrast the trans-differentiation as a result of c-Myc gain and loss of L-Myc
522 cells conferred sensitivity to Aurora Kinase A inhibition (*37*). The differential sensitivity
523 associated with distinct lineage state with Myc family member status as a biomarker could
524 translate to significant clinical implications in stratification of patients for targeted therapy (*50*).

525 SCLC is a recalcitrant disease typically characterized by neuroendocrine differentiation,
526 nonetheless approximately 10-20% of SCLCs may lack expression of diagnostic neuroendocrine
527 markers. Here we report, the plasticity between these histological subtypes and molecular
528 subtypes is regulated by c-Myc and L-Myc. The role in lineage determination and maintenance
529 for this family of transcription factors is striking since the Myc family has historically been
530 grouped as general oncogenes. Our data suggest that the role of Myc family in SCLC
531 tumorigenesis could be re-defined. This will enable us to categorize these subtypes to develop
532 effective therapies to combat this highly lethal disease.

533 **Methods**

534 *CCLE RNA-seq analysis*

535 RNA-seq gene expression data and SNP-array copy number data for *MYC*, *MYCL* and
536 *MYCN* were downloaded from (CCLE) web site. Log_2(RSEM (transcripts per million) +1) values
537 for mRNA expression and log_2(inferred copy number/2) values for copy numbers were used to
538 depict a heatmap for a 49 SCLC cell lines. *MYC* classified cell lines were further refined with
539 expression cut-off for *MYC* at log2 RSEM > 8 and expression of *MYCL* at log2 RSEM < 2. For
540 MYCL classified cell lines expression cut-off was set at *MYCL* log2 RSEM > 8 and expression
541 of *MYC* log2 RSEM < 2.

542

543 *Bayesian Network Analysis*

544 A comprehensive regulatory network was built using the software suite, Reconstructing
545 Integrative Molecular Bayesian Network (RIMBANet) (Zhu et al., 2004) by combining RNAseq
546 data from two independent SCLC primary cohorts (*21*, *25*) . To identify sub-networks enriched
547 for L-Myc and c-Myc signatures, the gene signature was overlaid on the network and
548 neighboring nodes within two layers for each signature were selected. Then closed subnetwork
549 with more than 25 nodes were collected for L-MYC and c-MYC subnetworks. Then, Key Driver
550 Analysis (*51*) identified master regulators associated with L-Myc and c-Myc signatures in two
551 steps. First, for each node in the network, we compared neighboring nodes within two layers for
552 each signature to obtain a list of potential master regulators whose overlap is statistical
553 significant (Fisher's exact test (FET) p-value<0.05/(# of nodes)). After sorting candidate genes
554 by corresponding FET p-values, the gene with the strongest p-value was determined as a key
555 regulator. Any candidate regulators in its two-layered neighbors were excluded from the

556 candidate list. The process was iterated throughout the sorted candidate list. Enriched functions
557 were identified using GO terms in Molecular Signatures Database (MSigDB). The significance
558 of the enrichment was determined based on FET p-value considering multiple testing (FET
559 $p<0.05/(\#\text{ of dataset tested})$) in each category.
560
561 *Cell Lines*
562 All cells were cultured at 37°C in a humidified incubator at 5% CO_2. SCLC cell lines
563 NCI-H2171, NCI-H82, NCI-H524, NCI-H209, NCI-H1963, PC-9, CORL88, HCC33, NCI-H69,
564 and NCI-H526 were maintained in RPMI1640 (Gibco), and supplemented with 10% Fetal
565 Bovine Serum (FBS, Sigma) and 1mM Penicillin Streptomycin (P/S, Gibco). HEK293T cells
566 were maintained in Dulbecco's Modified Eagle's Medium (DMEM), and supplemented with
567 10% FBS (Sigma) and 1mM P/S. HU-EV cells Cultured cells were regularly tested for
568 mycoplasma using the mycoAlert Detection Kit (Lonza).
569
570 *ATAC-seq*
571 ATAC-seq was performed as previously described (*52*). Five thousand cells were
572 harvested and pre-treated with DNase I (Thermo Fisher Scientific) at 37°C for 20 minutes to
573 eliminate DNA contamination from dead cells. The cells were washed in cold Phosphate-
574 buffered saline (PBS) to eliminate traces of DNase. Nuclei were isolated with nuclear lysis
575 buffer (10 mM Tris, 10mM NaCl, 3mM $MgCl_2$ 0.1% IGEPAL-630) and centrifuged at low
576 speeds. The nuclei were resuspended in transposase reaction mixture (10mM Tris PH 8.0, 5 mM
577 $MgCl_2$, 10% Dimethlyformamide (DMF), 0.2 mg/ml Tn5 transposase complex). Transposition
578 was carried out at 37°C for 30 minutes followed by DNA purification with DNA Clean and

579 Concentrator-25 (Zymo Research) according to manufacturer's recommendation. Following
580 purification, library fragments were PCR amplified with Nextera adapter primers. Sequencing
581 was performed at Tisch Cancer Institute sequencing core on the NextSeq500 (Illumina) for 38
582 nucleotides each from paired ends according to manufacturer's instructions.
583
584 *ATAC-seq data analysis*
585 Illumina sequencing adapter was removed using Cutadapt from raw sequence files in
586 fastq format. The reads were aligned to the hg19 reference genome using Bowtie2 with -k 1 and
587 default parameters. The aligned reads were used after removing PCR duplicates using Samtools
588 and filtered off an ATAC blacklist (*52*) for mitochondrial DNA and homologous sequences.
589 Both fragment ends were shifted +4 nucleotides for positive strand and -5 for negative strand to
590 account for distance from Tn5 binding and helicase activity to identify cut sites. Extended Tn5
591 cut sites were used for peak calling with MACS2 with parameters --nomodel --extsize 100 --shift
592 50 --nolambda --keep-dup all. Fraction of reads in peaks (FRiP) score was calculated for each
593 sample and was used as a normalization factor for pileup rescaled to a total number of uniquely
594 alignable sequences by WigMath function of Java-Genomic Toolkit. Peaks were filtered by
595 MYC motif using findMotifsGenome function in Homer using four motif matrices *MA0058.2*
596 *(MAX), MA0059.1 (MAX::MYC), MA0104.4 (MYCN), and MA0147.3 (MYC).* The peaks filtered
597 with MYC motifs were visualized in heatmaps by *k*-means clustering (*k*=8) using Cistrome ((*10*,
598 *35*) (*11*)) or using *k*-means clustering (*k*=6 for genetically engineered NCI-H1963 and *k*=4 for
599 genetically engineered NCI-H82 cells) using plotHeatmap function of deepTools (*53*) with
600 wiggle files. Normalized ATAC-seq signals for each sample was visualized on integrative
601 genome viewer (IGV) genome browser (*54*).

602 Differentially bound sites comparing three c-Myc classified cell lines vs three L-Myc
603 classified cell lines were identified using R package DiffBind with cutoffs at fold change ≥ 5 and
604 FDR ≤ 0.05. Functional analysis of the differentially bound regions was performed using
605 Genomic Regions Enrichment of Annotations Tool (GREAT)(*35*). For NCI-H82, differentially
606 bound sites were identified using R package DiffBind between 3 NCI-H82 control cells (LacZ,
607 LacZ/sgNT 1, and LacZ/sgNT2) and 3 c-Myc replaced by L-Myc (L-Myc/sg*MYC*1, L-
608 Myc/sg*MYC*2 and L-Myc/sg*MYC*3) with cutoffs at fold change > 16 and FDR <0.01. Functional
609 analysis of the differentially bound regions integrated with differentially expressed genes from
610 transcriptomic data of the same samples was performed using Cistrome-GO (*55*).
611
612 *Western Blot and Antibodies*
613 Protein lysates were prepared by washing cells with 1 ml of cold PBS and resuspended in
614 lysis buffer (150 mM NaCl, 50 mM Tris-HCl at pH 8.0, 1% NP-40, 0.5% Na deoxycholate, 0.1%
615 SDS, protease inhibitors) for 30 min at 4°C. Lysates were centrifuged at 5°C for 15 minutes at
616 13,000 rpm to remove insoluble debris. Protein concentrations were quantified using Pierce™
617 BCA (Thermo Fisher Scientific). Proteins were separated by electrophoresis on a SDS-PAGE gel
618 (BioRad), transferred to a PVDF membrane (Thermo Fisher Scientific) and blocked with 5%
619 milk in Tris-buffered saline with Tween-20 (TBS-T). The membranes were immunoblotted with
620 anti-c-Myc (sc-40, Santa Cruz Biotechnology), anti-L-Myc (PCRP-MYCL1-1A3, University of
621 Iowa), anti-vinculin (Sigma), anti-ASCL1 (#556604, BD Biosciences), anti-NeuroD1(12081-1-
622 AP, Proteintech), anti-Smad2 (#5339, Cell signaling technology), anti-Rest (07-579, Millipore
623 sigma), anti-Hes1 (sc-166410, Santa Cruz Biotechnology), anti-Brn2 (12137, Cell signaling

624 technology), anti-YAP1 (13584-1-AP, Proteintech) or anti-vinculin (Sigma). Immunoblots were
625 quantified using Image J.
626
627 *Lentiviral introduction of genes*
628 c-Myc, L-Myc or LacZ open reading frame (ORF) was cloned into pLEX_307 (a gift
629 from David Root, Addgene #41392) using the Gateway® cloning methods according to
630 manufacturer's recommendations. (Thermo Fisher Scientific). HEK293T cells were seeded in a
631 10 cm tissue culture dish and incubated at 37°C and 5% CO_2. At 80% confluency the cells were
632 co-transfected with 10 µg of plasmid constructs, 7.5 µg of psPAX2 (a gift from Didier Trono,
633 Addgene #12260) and 2.5 µg of pMD2.G (a gift from Didier Trono, Addgene #12259) vectors
634 using TransIT-Lenti (Mirus) following manufacturer's recommendations. At 48h post
635 transfection, virus-containing supernatants were collected, filtered (0.45 µm) and stored at
636 −80°C. Cells were infected with lentiviral supernatant supplemented with polybrene at a final
637 concentration of 8 µg/mL or lentiBlast (OZ BioSciences) at a ratio of 1:1000. Cells were selected
638 with puromycin (1-2 µg/mL for 4-6 days).
639
640 *CRISPR-Cas9 genome editing*
641 Cells with stable human codon-optimized S. pyogenes Cas9 expression were generated
642 by infection with the lentiCas9-Blast plasmid (a gift from Feng Zhang, Addgene # 52962).
643 sgRNAs targeting *MYC* and *MYCL* were selected from the Brunello library (*56*). Non-target
644 sgRNA from the Gecko library v2 (*57*) were used as non-target sgRNAs. sgGRNA target
645 sequences are listed in Supplementary Table S5. sgRNAs were cloned using BbsI site
646 downstream of the human U6 promoter in a lentiviral vector containing EGFP downstream of the

647 human PGK promoter (a kind gift of Brown laboratory, ISMMS). Lentivirus was produced as
648 described above. Cas9 expressing cells were then infected with pLenti-GFP-sgRNA.
649
650 *Cell proliferation assay*
651 Cells were plated at a density of 5,000 cells/well with five replicates in a 96-well plate;
652 four identical plates were prepared. Cell viability was assayed at 0, 2, 4 and 6 days after plating
653 with alamarBlue Cell Viability Reagent (Thermo Fisher Scientific) and fluorescence at 585 nm
654 was measured on a Spectra Max3 plate reader (Molecular Device) according to the
655 manufacturer's protocol at excitation of 555 nm. Cell viability at 2, 4 and 6 days were corrected
656 for the ratio to control cells from the day 0 reading to account for plating unevenness.
657
658 *RNA-seq*
659 Total RNAs from engineered NCI-H82 and NCI-H1963 cell lines were extracted using
660 RNeasy kit (Qiagen). Poly-adenylated RNA was enriched from 1ug of RNA for each sample
661 with the NEBNext® PolyA mRNA Magnetic Isolation Module (NEB), incubated at 94°C for 15
662 min and double-strand cDNA was synthesized using SuperScript III reverse transcriptase
663 (Thermo Fisher Scientific) and NEBNext® Ultra™ II Directional RNA Second Strand Synthesis
664 Module (NEB). Up to 10 ng of cDNA was used for the Illumina sequencing library construction
665 using NEBNext® Ultra™ DNA Library Prep Kit (NEB). Paired ends sequencing was performed
666 on NextSeq 500 (Illumina) for 38 nucleotides from each end according to the manufacturer's
667 instructions.
668
669 *RNA-seq analyses*

670 Sequencing reads were pseudoaligned to the human reference transcriptome GRCh38.95
671 from Ensembl and transcript abundance was estimated using kallisto (v0.45.0) (*58*). Transcript
672 abundance was aggregated to gene level abundance using biomaRt annotation. DEseq2 (*59*) was
673 used to identify differentially expressed genes between control NCI-H82 cells (LacZ,
674 LacZ/sgNT1, LacZ/sgNT2) and L-Myc-overexpressed NCI-H82 cells (L-Myc, L-Myc/sgNT1
675 and L-Myc/sgNT2). The same strategy was used for L-Myc-overexpressed NCI-H82 cells (L-
676 Myc, L-Myc/sgNT1 and L-Myc/sgNT2) and c-Myc replaced with L-Myc NCI-H82 cells (L-
677 Myc/sg*MYC*1, L-Myc/sg*MYC*2 and L-Myc/sg*MYC*3), as well as for LacZ-overexpressed NCI-
678 H1963 cells and c-Myc overexpressed NCI-H1963 cells.

679 Differentially expressed genes were determined based on cutoffs of fold change> 2 and
680 FDR<0.05. To identify potentially enriched functions of selected gene sets of interest, we
681 compared these gene sets with the genes annotated by Gene Ontology (GO) terms curated in the
682 Molecular Signature Database (MSigDB). Each of 5,917 GO terms included in "C5" collection
683 (version 7.0) was compared with query gene sets using Fisher's exact test. The significance of
684 the overlap was determined based on p-value adjusted for multiple comparisons (FDR<0.05).
685 Any GO terms consisting of more than 2,000 genes were considered non-specific and removed
686 from the analysis.

687

688 *Beta-galactosidase staining*

689 Cells were stained with beta-galactosidase FluoReporter™ Galactosidase Quantification
690 Kit (Thermo Fisher Scientific, F2905) according to manufacturer's recommendations in
691 technical triplicates.

692

693 *Cell cycle analysis*

694 Cells were harvested at day 2 after selection and fixed with 70 % ethanol overnight at
695 4°C, were washed with PBS, then, incubated in PBS containing 100 μg/ml RNase and 50 μg/ml
696 propidium iodide at room-temperature for 1 hour. DNA content was analyzed by FACS Canto II
697 (BD Bioscience), and quantitative analyses for the proportions of cells in cell cycle were
698 performed using FlowJo software (BD Bioscience).
699
700 *Annexin-V staining*
701 Cells were harvested at day 2 after selection and washed with PBS. Cells were stained
702 with Annexin-V and propidium iodide using Alexa Fluor® 488 annexin V/Dead Cell Apoptosis
703 Kit (Thermo Fisher Scientific) according to manufacturers' recommendations. Fluorescence was
704 measured by FACS Canto II (BD Bioscience). Quantitative analyses for the cell viability
705 proportions were performed using FlowJo software (BD Bioscience).
706
707 *Xenograft model*
708 All animal procedures and studies were approved by the Mount Sinai Institutional
709 Animal Care Use Committee (IACUC) (protocol number, IACUC-2018-0021). H1963 cells
710 which overexpressed LacZ or c-Myc (5 x 10^6 cells) were injected with a 1:1 mixture of 50 μl cell
711 suspension and 50 μl Matrigel (Corning) subcutaneously into both flank regions of 4- to 6-week-
712 old male NOD-scid gamma mice (Jackson Laboratory). Tumor volume (length x $width^2$ /2) was
713 measured twice a week. When tumor size reached at 1000 mm^3, mice were sacrificed and tumors
714 were immersed in formalin for histological analysis. Histopathology was reviewed by a board-
715 certified lung cancer pathologist (M. B. Beasley).
716
717 *Immunohistochemistry*

718 Xenograft tumor specimen formalin-fixed, paraffin-embedded tissue slides (5 μm thick)
719 were deparaffinized and rehydrated. For antigen-retrieval slides were heated at 95°C in 10 mM
720 citrate buffer (pH 6.0) for 30 minutes. The sections were incubated with 0.3% H_2O_2 in TBS for
721 15 minutes to block endogenous peroxidase activity and were incubated with 10% normal horse
722 serum (Jackson ImmunoResearch) in TBS for 30 minutes to block non-specific staining. The
723 sections were rinsed with TBS + 0.025% Triton X-100 and then incubated with anti-cMYC
724 antibody (1:150; Abcam #ab32072), anti-NeuroD1 (1:1000, Abcam #ab60704) or anti-ASCL1
725 (1:100, BD Biosciences #556604) at 4°C overnight. This was followed by incubation with
726 biotin-conjugated Horse anti-Mouse secondary antibody (Vector Laboratories) at room
727 temperature for 1 hour. Then, the sections were incubated with the ABC reagent (Vector
728 Laboratories, CA) and visualized with ImmPACT-DAB Peroxidase Substrate (Vector
729 Laboratories). All slides were counterstained with hematoxylin before being mounting.
730
731 *Aurora Kinase Inhibition Assay*
732 Cells were seeded in a 96-well plate at a density of 5,000 cells/well with five replicates. Cells
733 were treated with Alisertib at concentrations ranging from 1 nM to 10 μM for 96h. Cell viability
734 was measured using alamarBlue Cell Viability Reagent (Thermo Fisher Scientific) and
735 fluorescence at 585nm was measured on a Spectra Max3 plate reader (Molecular Devices, CA)
736 according to the manufacturer's protocol at excitation of 555 nm.
737
738 *Chromatin immunoprecipitation followed by quantitative PCR*

739 Chromatin immunoprecipitation was performed as previously described (ref). $1x10^7$ cells
740 were crosslinked with 1% formaldehyde in PBS for 10 minutes at room temperature, washed in 5

741 mg/mL BSA in PBS and then in just cold PBS, resuspended in lysis buffer [50 mmol/L Tris-HCl
742 pH 8.1, 10 mmol/L EDTA, 1% SDS, 1 × protease inhibitor cocktail (Thermo Fisher Scientific)]
743 and sonicated with the Covaris M220 sonicator to obtain chromatin fragment lengths of 100-to-
744 1,000 bp judged by Bioanalyzer DNA High Sensitivity Kit (Agilent). Fragmented chromatin was
745 diluted in immunoprecipitation (IP) buffer (20 mmol/L Tris-HCl pH 8.1, 150 mmol/L NaCl, 2
746 mmol/L EDTA, 1% Triton X-100) and incubated overnight at 4°C with protein G magnetic
747 beads (Dynabeads, Thermo Fisher Scientific) that had been preincubated with anti-MYC (#9402,
748 Cell signaling technology) or anti-REST (07-579, Millipore Sigma) antibodies.
749 Immunoprecipitates were washed six times with the wash buffer (50 mmol/L HEPES pH 7.6, 0.5
750 mol/L LiCl, 1 mmol/L EDTA, 0.7% sodium deoxycholate, 1% IGEPAL CA-630) and twice with
751 Tris-EDTA buffer. Immunoprecipitated (or no IP input) DNA was treated with RNase A and
752 Proteinase K on the beads, recovered in 1% SDS and 0.1 mol/L $NaHCO_3$ over a period of 7
753 hours at 65°C, and purified with DNA clean and concentrator-25 (Zymo Research).
754 Real-time quantitative PCRs were performed in duplicate (Applied Biosystems) on a
755 7500 Real-Time PCR System (Applied Biosystems) with results normalized to input. Primers are
756 listed in Supplementary Table S6.

757 *Quantitative reverse transcription PCR*

758 For expression analysis, RNA was extracted from cells using the Qiagen RNeasy Mini
759 Kit and cDNA was prepared with the Qiagen QuantiTect Reverse Transcription Kit. Real-time
760 quantitative PCRs were performed as described above with results normalized
761 to *GAPDH* expression. Primers are listed in Supplementary Table S6.

762 **Acknowledgements**

763 We thank Dawei Yang, Feng Jiang, Yang Tian, Bhavana Shewale, Nicole Stokes, David
764 Dominique-Sola, Yifei Sun for helpful discussions and technical assistance. Christie Nguyen and
765 Emily Bernstein for providing the Rest antibody, Peipei Guo for providing HU-EV cells.
766 Aleksandra Wroblewska and Brian D. Brown for providing a lentiviral vector for cloning
767 sgRNAs; NextSeq Sequencing Facility of the Department of Oncological Sciences at Icahn
768 School of Medicine at Mount Sinai (ISMMS), Saboor Hekmaty, Gayatri Panda and Ravi
769 Sachidanandam for sequencing assistance. The authors also thank the Flow Cytometry Core
770 facility and the Biorepository and Pathology Core Facility at ISMMS. This work was supported
771 in part through Tisch Cancer Institute at ISMMS and the computational resources and staff
772 expertise provided by Scientific Computing at ISMMS. H. Watanabe has been supported by ATS
773 Foundation Unrestricted Grant, the American Lung Association of the Northeast Lung Cancer
774 Discovery Award, Department of Defense (W81XWH-19-1-0613) and NIH (R01CA240342). T.
775 Sato is supported by the Japanese Respiratory Society the 6th Lilly Oncology Fellowship
776 Program and the Uehara Memorial Foundation. R. Kong is supported by Shaanxi Provincial
777 Natural Science Foundation, China (2017JM8046). C.A. Powell and H. Watanabe are supported
778 by NIH (R01CA163772).

779 **Author Contribution**

780 Conceptualization & Methodology, A.S.P. and H.W.; Data Collection: A.S.P., S.Y., R.K., T.S.,
781 A.S., S.K., L.B., M.F., K.E. and H.W.; Resources, M.B.B., C.A.P. and H.W.; Data Analysis,
782 A.S.P., S.Y., G.N., M.B.B. and H.W.; Writing – Original Draft, A.S.P. and H.W.; Writing –
783 Review & Editing, A.S.P., S.Y., C.A.P., M.B.B, J.Z. and H.W.; Supervision, C.A.P., J.Z. and
784 H.W.; Project Administration & Funding Acquisition, H.W.
785

786

787 **Data and Materials Availability**

788 All data needed to evaluate the conclusions in the paper are present in the paper and/or the
789 Supplementary Materials. Additional data may be available from authors upon request. The
790 sequencing data have been deposited into GEO with the accession number GSE156334.

791

792 **Declaration of Interests**

793 J. Zhu is the head of data science and S. Yoo is an employee at Sema4 Genomics, a Mount Sinai
794 venture, a for-profit organization that promotes genomic sequencing for patient-centered
795 healthcare.

796 **Figure legends**

797 **Figure 1:** Bayesian network analysis reveals unique L-Myc and c-Myc networks associated with
798 distinct biological processes

799 A. Schematic of workflow to use SCLC Bayesian causal gene regulatory network to identify
800 networks involving c-Myc and L-Myc.

801 B. L-Myc sub-network showing directionality and association of genes when L-Myc gene
802 signature (Figure S1C, Table S1) is projected to SCLC Bayesian network. Circles colored
803 in pink represent nodes from L-Myc gene signature. Size of pink circles is directly
804 proportional to the number of outgoing nodes. Nodes indicated in larger text are Key
805 drivers of the sub-network (Table S2).

806 C. Gene Ontology analysis for L-Myc neighbor subnetwork. Enriched functions for these
807 genes are identified based on hypergeometric test against GO terms.

808 D. Three c-Myc sub-networks showing directionality and association of genes when c-Myc
809 associated gene signature (Figure S1C, Table S1) is projected to SCLC Bayesian
810 network. Circles colored in blue represent nodes from c-Myc gene signature. Size of blue
811 circles is directly proportional to the number of outgoing nodes. Nodes indicated in larger
812 text are Key drivers of the sub-network (Table S3).

813 E. Gene Ontology analysis for corresponding c-Myc neighbor subnetwork. Enriched
814 functions for these genes are identified based on hypergeometric test against GO terms.

815

816 **Figure 2:** c-Myc and L-Myc driven SCLCs exhibit distinct chromatin states to regulate distinct
817 transcriptional programs

818 A. Protein expression of c-Myc and L-Myc as well as vinculin as a loading control in a panel
819 of representative SCLC cell lines (blue: c-MYC-classified lines, pink: L-MYC-
820 classified lines)
821 B. Schematic showing the analytic approach to define MYC accessible regions.
822 C. Principal component analysis of open chromatin regions with E-Box motif in six
823 SCLC cell lines. Each dot represents a SCLC cell line that is colored based on Myc
824 status (blue: c-Myc-classified cell lines, pink: L-Myc-classified cell lines).
825 D. Each heatmap depicting global MYC (E-box) accessibility in individual SCLC cell
826 lines at 72,833 combined peaks. ATAC-seq signal intensity is shown by color shading.
827 E. Genome browser view tracks of ATAC-seq signals at the *FOXA2* and *ITGA4* loci (pink:
828 L-Myc-classified cell lines, blue: c-Myc-classified cell lines).
829 F. Heatmap showing 2,808 differentially accessible regions (fold change ≥ 5 and FDR ≤
830 0.05) between 3 L-Myc cell lines shown in pink and 3 c-Myc cell lines shown in blue.
831 G. Enriched ontology by GREAT analyses for regions differentially accessible in L-Myc
832 classified cells.
833 H. Enriched ontology by GREAT analyses for regions differentially accessible in c-Myc
834 classified cells.
835
836 **Figure 3:** c-Myc and L-Myc expression is associated with distinct molecular subtype markers
837 A. Unsupervised clustering of 137 primary tumors and 51 CCLE cell lines using the
838 expression of ASCL1, NeuroD1, POU2F3 and YAP1 distinguishing four molecular
839 subtypes (Table S4).

840 B. Box plot showing mRNA expression of L-Myc across four molecular subtypes for
841 combined primary tumor and cell line classification described in Figure 3A.
842 C. Box plot showing mRNA expression of c-Myc across four molecular subtypes for
843 combined primary tumor and cell line classification described in Figure 3A.
844 D. Scatter-plot with best-fit line showing negative correlation between c-Myc and ASCL1
845 expression for combined primary tumor and cell lines. Pearson's correlation coefficient
846 (r) = -0.53, P <0.01 t-test.
847
848 **Figure 4:** L-Myc induces neuronal state not defined by ASCL1 expression
849 A. Workflow schematic to genetically engineer replacement of c-Myc with L-Myc.
850 B. Protein expression of L-Myc, c-Myc, ASCL1, NeuroD1 and YAP1, with vinculin as
851 loading control in replaced NCI-H82 cells. Quantified in Figure S5A.
852 C. Cell growth curve for genetically engineered NCI-H82 cells. **, P <0.01 vs. Lac-Z/sgNT
853 NCI-H82 cells, t-test.
854 D. Protein expression of c-Myc and NeuroD1 with vinculin as loading control in NCI-H82
855 cells with c-Myc ablation. Quantified in Figure S5F.
856 E. Volcano plot showing 1,213 differentially expressed genes (713 upregulated in pink and
857 500 downregulated in blue). NCI-H82 (LacZ and LacZ/sgNT) vs NCI-H82
858 (LMYC/sg*MYC*).
859 F. Ridgeplot showing distribution of fold-change for genes in each enriched gene ontology
860 term for upregulated genes (Figure 4E).

861 G. PCA of 14 SCLC cell lines, including 3 ASCL1, 2 NEUROD1 and 9 genetically
862 engineered NCI-H82 cells, 3 control (LacZ or LacZ/sgNT), 3 L-Myc overexpressed (L-
863 Myc and L-Myc/sgNT) and 3 c-Myc replaced with L-Myc (L-Myc/sg*MYC*).
864 H. Each heatmap depicting *k-means* (k =4) clustering of global Myc accessibility in NCI-
865 H82 LacZ/sgNT (left) and NCI-H82 L-MYC/sgMYC (right) at 170,711 combined
866 peaks. ATAC-seq signal intensity is shown by color shading.
867 I. Heatmap showing 2,807 differentially accessible regions (fold change > 16 and FDR
868 <0.01) between 3 NCI-H82 control cells (LacZ and LacZ/sgNT) and 3 c-Myc replaced by
869 L-Myc (L-Myc/sg*MYC*)
870 J. Enriched ontology by Cistrome-GO analyses for regions Myc accessible regions gained
871 (top) and lost (bottom) after replacement.
872
873 **Figure 5:** c-Myc expression in ASCL1-subtype SCLC induces trans-differentiation to
874 histologically distinct NeuroD1-positive state
875 A-B. Protein expression of c-Myc, L-Myc, ASCL1, and NeuroD1, as well as vinculin as
876 loading control in genetically engineered NCI-H1963 (A) and NCI-H187 (B) cells.
877 Quantification in Figure S8A (NCI-H1963) and S8B (NCI-H187).
878 C-D. Cell growth curve for NCI-H1963 (C) and NCI-H187 (D) cells with over-expression of
879 c-Myc or control Lac-Z. Mean ± SD of five technical replicates. **, P <0.01 vs. Lac-Z
880 overexpressed control cells, t-test.
881 E. Bar chart shows proportions of viable, necrotic and apoptotic cells in NCI-H1963 c-Myc
882 overexpressed and control cells measured by Annexin-V staining. Mean ± SD of three
883 biological replicates. ** $P < 0.01$, t-test. Scatter plots shown in Figure S8E.

884 F. Hematoxylin-eosin staining and immunohistochemical staining of c-Myc, ASCL1 and
885 NeuroD1 in LacZ-overexpressed (top panel) or c-Myc-overexpressed (bottom panel)
886 NCI-H1963 xenograft. H&E original images, x600 and IHC original images, x20.
887 G. Hematoxylin-eosin staining of typical SCLC and LCNEC primary human tumors.
888 Original images, x400.
889
890 **Figure 6:** c-Myc rewires Myc-accessible chromatin regulatory elements to regulate distinct
891 lineage associated pathways
892 A. Each heatmap depicting *k-means* (k =6) clustering of global Myc (E-box) accessibility
893 in NCI-H1963 overexpressing LacZ (left) and NCI-H1963 overexpressing cMYC (right)
894 at 44,722 combined peaks. ATAC-seq signal intensity is shown by color shading.
895 B. Principal component analysis of open chromatin regions with E-Box motif in six
896 SCLC cell lines in addition to NCI-H1963-LacZ (control) and NCI-H1963-c-Myc in
897 triplicate. Each dot represents a SCLC cell line that is colored based on Myc status
898 (pink: L-MYC, blue: c-MYC, red: NCI-H1963 LacZ, light blue: NCI-H1963 cMYC).
899 C. Volcano plot showing 775 differentially expressed genes (375 upregulated in light blue
900 and 400 downregulated in red) between control NCI-H1963 cells with LacZ-
901 overexpression cells and NCI-H1963 cells with c-Myc-overexpression.
902 D. Dot plot showing gene ontology analysis for differentially upregulated (right panel) and
903 downregulated (left panel) genes.
904
905 **Figure 7:** c-Myc induces neuronal repressor REST to mediates lineage conversion

906 A. Expression of *REST* in NCI-H1963 cells with LacZ over-expression and NCI-H1963 with
907 c-Myc overexpression (n =3).
908 B. Protein expression of c-Myc, and Rest, as well as vinculin as loading control in
909 genetically engineered NCI-H1963 cells.
910 C. Protein expression of Rest, ASCL1, as well as vinculin as a loading control in genetically
911 engineered NCI-H1963 cells to overexpress Rest.
912 D. Protein expression of c-Myc, Rest, and ASCL1 as well as vinculin as a lading control in
913 genetically engineered NCI-H1963 cells genetically deleted for REST and over-
914 expressed with either LacZ as control or c-Myc.
915 E. Protein expression of c-Myc, L-Myc, ASCL1, and Rest, as well as vinculin as loading
916 control in genetically engineered NCI-H1963 cells treated with vehicle (DMSO) or 10
917 μM of a Rest inhibitor (X5050) for 48 hours.
918 F. REST ChIP-qPCR in NCI-H1963 c-Myc overexpressed cells and LacZ overexpressed
919 cells (negative control) at the *ASCL1* and *MYCL* loci with *7q31* and *HOPX* as negative
920 control loci. One representative of three biological replicates is shown.
921 G. Protein expression of c-Myc, L-Myc, ASCL1, and Rest, as well as vinculin as loading
922 control in genetically engineered NCI-H1963 cells treated with vehicle (DMSO) or 0.5
923 μM of a Notch inhibitor (DBZ) for 48 hours.
924 H. Protein expression of c-Myc, L-Myc, ASCL1, and Rest, as well as vinculin as loading
925 control in genetically engineered NCI-H1963 cells treated with vehicle (DMSO) or 10
926 μM of a Notch inhibitor (DAPT) for 48 hours.

927 I. c-Myc ChIP-qPCR in NCI-H1963 c-Myc overexpressed cells and LacZ overexpressed
928 cells (negative control) at the *ASCL1* and *REST* loci with *7q31* and *HOPX* as negative
929 control loci. One representative of three biological replicates is shown.
930 J. Graphical schematic representing role of c-Myc and L-Myc as lineage determining
931 factors in SCLC.

932 **References**
933

934 1. R. L. Siegel, K. D. Miller, A. Jemal, Cancer statistics, 2019. *CA. Cancer J. Clin.* **69**, 7–34
935 (2019).

936 2. A. F. Gazdar, P. A. Bunn, J. D. Minna, Small-cell lung cancer: what we know, what we
937 need to know and the path forward. *Nat. Rev. Cancer*. **17**, 725–737 (2017).

938 3. G. Alvarado-Luna, D. Morales-Espinosa, Treatment for small cell lung cancer, where are
939 we now?-a review. *Transl. Lung Cancer Res.* **5**, 26–38 (2016).

940 4. M. C. Pietanza, L. A. Byers, J. D. Minna, C. M. Rudin, Small Cell Lung Cancer: Will
941 Recent Progress Lead to Improved Outcomes? *Clin. Cancer Res.* **21**, 2244–2255 (2015).

942 5. L. Horn, A. S. Mansfield, A. Szczęsna, L. Havel, M. Krzakowski, M. J. Hochmair, F.
943 Huemer, G. Losonczy, M. L. Johnson, M. Nishio, M. Reck, T. Mok, S. Lam, D. S. Shames,
944 J. Liu, B. Ding, A. Lopez-Chavez, F. Kabbinavar, W. Lin, A. Sandler, S. V. Liu, First-Line
945 Atezolizumab plus Chemotherapy in Extensive-Stage Small-Cell Lung Cancer. *N. Engl. J.*
946 *Med.* **379**, 2220–2229 (2018).

947 6. C. M. Rudin, J. T. Poirier, L. A. Byers, C. Dive, A. Dowlati, J. George, J. V. Heymach, J.
948 E. Johnson, J. M. Lehman, D. MacPherson, P. P. Massion, J. D. Minna, T. G. Oliver, V.
949 Quaranta, J. Sage, R. K. Thomas, C. R. Vakoc, A. F. Gazdar, Molecular subtypes of small
950 cell lung cancer: a synthesis of human and mouse model data. *Nat. Rev. Cancer.* **19**, 289–
951 297 (2019).

952 7. C. Zappa, S. A. Mousa, Non-small cell lung cancer: current treatment and future advances.
953 *Transl. Lung Cancer Res.* **5**, 288–300 (2016).

954 8. D. N. Carney, A. F. Gazdar, G. Bepler, J. G. Guccion, P. J. Marangos, T. W. Moody, M. H.
955 Zweig, J. D. Minna, Establishment and Identification of Small Cell Lung Cancer Cell Lines
956 Having Classic and Variant Features. *Cancer Res.* **45**, 2913 (1985).

957 9. A. F. Gazdar, D. N. Carney, M. M. Nau, J. D. Minna, Characterization of Variant
958 Subclasses of Cell Lines Derived from Small Cell Lung Cancer Having Distinctive
959 Biochemical, Morphological, and Growth Properties. *Cancer Res.* **45**, 2924 (1985).

960 10. W. D. Travis, E. Brambilla, A. G. Nicholson, Y. Yatabe, J. H. M. Austin, M. B. Beasley,
961 Lucian. R. Chirieac, S. Dacic, E. Duhig, D. B. Flieder, K. Geisinger, F. R. Hirsch, Y.
962 Ishikawa, K. M. Kerr, M. Noguchi, G. Pelosi, C. A. Powell, M. S. Tsao, I. Wistuba, The
963 2015 World Health Organization Classification of Lung Tumors. *J. Thorac. Oncol.* **10**,
964 1243–1260 (2015).

965 11. J. T. Poirier, I. Dobromilskaya, W. F. Moriarty, C. D. Peacock, C. L. Hann, C. M. Rudin,
966 Selective Tropism of Seneca Valley Virus for Variant Subtype Small Cell Lung Cancer.
967 *JNCI J. Natl. Cancer Inst.* **105**, 1059–1065 (2013).

968 12. M. D. Borromeo, T. K. Savage, R. K. Kollipara, M. He, A. Augustyn, J. K. Osborne, L.
969 Girard, J. D. Minna, A. F. Gazdar, M. H. Cobb, J. E. Johnson, ASCL1 and NEUROD1
970 Reveal Heterogeneity in Pulmonary Neuroendocrine Tumors and Regulate Distinct Genetic
971 Programs. *Cell Rep.* **16**, 1259–1272 (2016).

972 13. K. McColl, G. Wildey, N. Sakre, M. B. Lipka, M. Behtaj, A. Kresak, Y. Chen, M. Yang, V.
973 Velcheti, P. Fu, A. Dowlati, Reciprocal expression of INSM1 and YAP1 defines subgroups
974 in small cell lung cancer. *Oncotarget*. **8** (2017), doi:10.18632/oncotarget.20572.

975 14. Y.-H. Huang, O. Klingbeil, X.-Y. He, X. S. Wu, G. Arun, B. Lu, T. D. D. Somerville, J. P.
976 Milazzo, J. E. Wilkinson, O. E. Demerdash, D. L. Spector, M. Egeblad, J. Shi, C. R. Vakoc,
977 POU2F3 is a master regulator of a tuft cell-like variant of small cell lung cancer. *Genes*
978 *Dev.* **32**, 915–928 (2018).

979 15. J. Brägelmann, S. Böhm, M. R. Guthrie, G. Mollaoglu, T. G. Oliver, M. L. Sos, Family
980 matters: How MYC family oncogenes impact small cell lung cancer. *Cell Cycle*. **16**, 1489–
981 1498 (2017).

982 16. D.-W. Kim, N. Wu, Y.-C. Kim, P. F. Cheng, R. Basom, D. Kim, C. T. Dunn, A. Y. Lee, K.
983 Kim, C. S. Lee, A. Singh, A. F. Gazdar, C. R. Harris, R. N. Eisenman, K.-S. Park, D.
984 MacPherson, Genetic requirement for *Mycl* and efficacy of RNA Pol I inhibition in mouse
985 models of small cell lung cancer. *Genes Dev.* **30**, 1289–1299 (2016).

986 17. R. Meuwissen, S. C. Linn, R. I. Linnoila, J. Zevenhoven, W. J. Mooi, A. Berns, Induction
987 of small cell lung cancer by somatic inactivation of both Trp53 and Rb1 in a conditional
988 mouse model. *Cancer Cell*. **4**, 181–189 (2003).

989 18. G. Mollaoglu, M. R. Guthrie, S. Böhm, J. Brägelmann, I. Can, P. M. Ballieu, A. Marx, J.
990 George, C. Heinen, M. D. Chalishazar, H. Cheng, A. S. Ireland, K. E. Denning, A.
991 Mukhopadhyay, J. M. Vahrenkamp, K. C. Berrett, T. L. Mosbruger, J. Wang, J. L. Kohan,
992 M. E. Salama, B. L. Witt, M. Peifer, R. K. Thomas, J. Gertz, J. E. Johnson, A. F. Gazdar, R.
993 J. Wechsler-Reya, M. L. Sos, T. G. Oliver, MYC Drives Progression of Small Cell Lung
994 Cancer to a Variant Neuroendocrine Subtype with Vulnerability to Aurora Kinase
995 Inhibition. *Cancer Cell*. **31**, 270–285 (2017).

996 19. R. DePinho, L. Mitsock, K. Hatton, P. Ferrier, K. Zimmerman, E. Legouy, A. Tesfaye, R.
997 Collum, G. Yancopoulos, P. Nisen, R. Kriz, F. Alt, Myc family of cellular oncogenes. *J.*
998 *Cell. Biochem.* **33**, 257–266 (1987).

999 20. M. Conacci-Sorrell, L. McFerrin, R. N. Eisenman, An Overview of MYC and Its
1000 Interactome. *Cold Spring Harb. Perspect. Med.* **4**, a014357–a014357 (2014).

1001 21. J. George, J. S. Lim, S. J. Jang, Y. Cun, L. Ozretić, G. Kong, F. Leenders, X. Lu, L.
1002 Fernández-Cuesta, G. Bosco, C. Müller, I. Dahmen, N. S. Jahchan, K.-S. Park, D. Yang, A.
1003 N. Karnezis, D. Vaka, A. Torres, M. S. Wang, J. O. Korbel, R. Menon, S.-M. Chun, D.
1004 Kim, M. Wilkerson, N. Hayes, D. Engelmann, B. Pützer, M. Bos, S. Michels, I. Vlasic, D.
1005 Seidel, B. Pinther, P. Schaub, C. Becker, J. Altmüller, J. Yokota, T. Kohno, R. Iwakawa, K.
1006 Tsuta, M. Noguchi, T. Muley, H. Hoffmann, P. A. Schnabel, I. Petersen, Y. Chen, A.

1007 Soltermann, V. Tischler, C. Choi, Y.-H. Kim, P. P. Massion, Y. Zou, D. Jovanovic, M.
1008 Kontic, G. M. Wright, P. A. Russell, B. Solomon, I. Koch, M. Lindner, L. A. Muscarella,
1009 A. la Torre, J. K. Field, M. Jakopovic, J. Knezevic, E. Castaños-Vélez, L. Roz, U.
1010 Pastorino, O.-T. Brustugun, M. Lund-Iversen, E. Thunnissen, J. Köhler, M. Schuler, J.
1011 Botling, M. Sandelin, M. Sanchez-Cespedes, H. B. Salvesen, V. Achter, U. Lang, M.
1012 Bogus, P. M. Schneider, T. Zander, S. Ansén, M. Hallek, J. Wolf, M. Vingron, Y. Yatabe,
1013 W. D. Travis, P. Nürnberg, C. Reinhardt, S. Perner, L. Heukamp, R. Büttner, S. A. Haas, E.
1014 Brambilla, M. Peifer, J. Sage, R. K. Thomas, Comprehensive genomic profiles of small cell
1015 lung cancer. *Nature*. **524**, 47–53 (2015).

1016 22. B. A. Weir, M. S. Woo, G. Getz, S. Perner, L. Ding, R. Beroukhim, W. M. Lin, M. A.
1017 Province, A. Kraja, L. A. Johnson, K. Shah, M. Sato, R. K. Thomas, J. A. Barletta, I. B.
1018 Borecki, S. Broderick, A. C. Chang, D. Y. Chiang, L. R. Chirieac, J. Cho, Y. Fujii, A. F.
1019 Gazdar, T. Giordano, H. Greulich, M. Hanna, B. E. Johnson, M. G. Kris, A. Lash, L. Lin,
1020 N. Lindeman, E. R. Mardis, J. D. McPherson, J. D. Minna, M. B. Morgan, M. Nadel, M. B.
1021 Orringer, J. R. Osborne, B. Ozenberger, A. H. Ramos, J. Robinson, J. A. Roth, V. Rusch,
1022 H. Sasaki, F. Shepherd, C. Sougnez, M. R. Spitz, M.-S. Tsao, D. Twomey, R. G. W.
1023 Verhaak, G. M. Weinstock, D. A. Wheeler, W. Winckler, A. Yoshizawa, S. Yu, M. F.
1024 Zakowski, Q. Zhang, D. G. Beer, I. I. Wistuba, M. A. Watson, L. A. Garraway, M.
1025 Ladanyi, W. D. Travis, W. Pao, M. A. Rubin, S. B. Gabriel, R. A. Gibbs, H. E. Varmus, R.
1026 K. Wilson, E. S. Lander, M. Meyerson, Characterizing the cancer genome in lung
1027 adenocarcinoma. *Nature*. **450**, 893–898 (2007).

1028 23. The Cancer Genome Atlas Research Network, Comprehensive genomic characterization of
1029 squamous cell lung cancers. *Nature*. **489**, 519–525 (2012).

1030 24. A. S. Ireland, A. M. Micinski, D. W. Kastner, B. Guo, S. J. Wait, K. B. Spainhower, C. C.
1031 Conley, O. S. Chen, M. R. Guthrie, D. Soltero, Y. Qiao, X. Huang, S. Tarapcsák, S.
1032 Devarakonda, M. D. Chalishazar, J. Gertz, J. C. Moser, G. Marth, S. Puri, B. L. Witt, B. T.
1033 Spike, T. G. Oliver, MYC Drives Temporal Evolution of Small Cell Lung Cancer Subtypes
1034 by Reprogramming Neuroendocrine Fate. *Cancer Cell*. **38**, 60-78.e12 (2020).

1035 25. L. Jiang, J. Huang, B. W. Higgs, Z. Hu, Z. Xiao, X. Yao, S. Conley, H. Zhong, Z. Liu, P.
1036 Brohawn, D. Shen, S. Wu, X. Ge, Y. Jiang, Y. Zhao, Y. Lou, C. Morehouse, W. Zhu, Y.
1037 Sebastian, M. Czapiga, V. Oganesyan, H. Fu, Y. Niu, W. Zhang, K. Streicher, D. Tice, H.
1038 Zhao, M. Zhu, L. Xu, R. Herbst, X. Su, Y. Gu, S. Li, L. Huang, J. Gu, B. Han, B. Jallal, H.
1039 Shen, Y. Yao, Genomic Landscape Survey Identifies SRSF1 as a Key Oncodriver in Small
1040 Cell Lung Cancer. *PLOS Genet.* **12**, e1005895 (2016).

1041 26. J. Zhu, P. Y. Lum, J. Lamb, D. GuhaThakurta, S. W. Edwards, R. Thieringer, J. P. Berger,
1042 M. S. Wu, J. Thompson, A. B. Sachs, E. E. Schadt, An integrative genomics approach to
1043 the reconstruction of gene networks in segregating populations. *Cytogenet. Genome Res.*
1044 **105**, 363–374 (2004).

1045 27. J. Zhu, B. Zhang, E. N. Smith, B. Drees, R. B. Brem, L. Kruglyak, R. E. Bumgarner, E. E.
1046 Schadt, Integrating large-scale functional genomic data to dissect the complexity of yeast
1047 regulatory networks. *Nat. Genet.* **40**, 854–861 (2008).

1048 28. W. Zhang, L. Girard, Y.-A. Zhang, T. Haruki, M. Papari-Zareei, V. Stastny, H. K. Ghayee,
1049 K. Pacak, T. G. Oliver, J. D. Minna, A. F. Gazdar, Small cell lung cancer tumors and
1050 preclinical models display heterogeneity of neuroendocrine phenotypes. *Transl. Lung*
1051 *Cancer Res.* **7**, 32–49 (2018).

1052 29. J. S. Lim, A. Ibaseta, M. M. Fischer, B. Cancilla, G. O'Young, S. Cristea, V. C. Luca, D.
1053 Yang, N. S. Jahchan, C. Hamard, M. Antoine, M. Wislez, C. Kong, J. Cain, Y.-W. Liu, A.
1054 M. Kapoun, K. C. Garcia, T. Hoey, C. L. Murriel, J. Sage, Intratumoural heterogeneity
1055 generated by Notch signalling promotes small-cell lung cancer. *Nature*. **545**, 360–364
1056 (2017).

1057 30. C. M. Rudin, S. Durinck, E. W. Stawiski, J. T. Poirier, Z. Modrusan, D. S. Shames, E. A.
1058 Bergbower, Y. Guan, J. Shin, J. Guillory, C. S. Rivers, C. K. Foo, D. Bhatt, J. Stinson, F.
1059 Gnad, P. M. Haverty, R. Gentleman, S. Chaudhuri, V. Janakiraman, B. S. Jaiswal, C.
1060 Parikh, W. Yuan, Z. Zhang, H. Koeppen, T. D. Wu, H. M. Stern, R. L. Yauch, K. E.
1061 Huffman, D. D. Paskulin, P. B. Illei, M. Varella-Garcia, A. F. Gazdar, F. J. de Sauvage, R.
1062 Bourgon, J. D. Minna, M. V. Brock, S. Seshagiri, Comprehensive genomic analysis
1063 identifies SOX2 as a frequently amplified gene in small-cell lung cancer. *Nat. Genet.* **44**,
1064 1111–1116 (2012).

1065 31. C. Y. Lin, J. Lovén, P. B. Rahl, R. M. Paranal, C. B. Burge, J. E. Bradner, T. I. Lee, R. A.
1066 Young, Transcriptional Amplification in Tumor Cells with Elevated c-Myc. *Cell*. **151**, 56–
1067 67 (2012).

1068 32. H. Wan, Foxa2 regulates alveolarization and goblet cell hyperplasia. *Development*. **131**,
1069 953–964 (2004).

1070 33. A. L. M. Ferri, W. Lin, Y. E. Mavromatakis, J. C. Wang, H. Sasaki, J. A. Whitsett, S.-L.
1071 Ang, Foxa1 and Foxa2 regulate multiple phases of midbrain dopaminergic neuron
1072 development in a dosage-dependent manner. *Dev. Camb. Engl.* **134**, 2761–2769 (2007).

1073 34. T. Sato, S. Yoo, R. Kong, A. Sinha, P. Chandramani-Shivalingappa, A. Patel, M. Fridrikh,
1074 O. Nagano, T. Masuko, M. B. Beasley, C. A. Powell, J. Zhu, H. Watanabe, *Cancer Res.*, in
1075 press, doi:10.1158/0008-5472.CAN-19-2132.

1076 35. C. Y. McLean, D. Bristor, M. Hiller, S. L. Clarke, B. T. Schaar, C. B. Lowe, A. M. Wenger,
1077 G. Bejerano, GREAT improves functional interpretation of cis-regulatory regions. *Nat.*
1078 *Biotechnol.* **28**, 495–501 (2010).

1079 36. M. Jain, Sustained Loss of a Neoplastic Phenotype by Brief Inactivation of MYC. *Science*.
1080 **297**, 102–104 (2002).

1081 37. M. A. Dammert, J. Brägelmann, R. R. Olsen, S. Böhm, N. Monhasery, C. P. Whitney, M.
1082 D. Chalishazar, H. L. Tumbrink, M. R. Guthrie, S. Klein, A. S. Ireland, J. Ryan, A. Schmitt,
1083 A. Marx, L. Ozretić, R. Castiglione, C. Lorenz, R. D. Jachimowicz, E. Wolf, R. K. Thomas,
1084 J. T. Poirier, R. Büttner, T. Sen, L. A. Byers, H. C. Reinhardt, A. Letai, T. G. Oliver, M. L.
1085 Sos, MYC paralog-dependent apoptotic priming orchestrates a spectrum of vulnerabilities
1086 in small cell lung cancer. *Nat. Commun.* **10**, 3485 (2019).

1087 38. C. V. Dang, MYC on the Path to Cancer. *Cell*. **149**, 22–35 (2012).

1088 39. N. Rekhtman, Neuroendocrine tumors of the lung: an update. *Arch. Pathol. Lab. Med.* **134**,
1089 1628–1638 (2010).

1090 40. J. George, V. Walter, M. Peifer, L. B. Alexandrov, D. Seidel, F. Leenders, L. Maas, C.
1091 Müller, I. Dahmen, T. M. Delhomme, M. Ardin, N. Leblay, G. Byrnes, R. Sun, A. De
1092 Reynies, A. McLeer-Florin, G. Bosco, F. Malchers, R. Menon, J. Altmüller, C. Becker, P.
1093 Nürnberg, V. Achter, U. Lang, P. M. Schneider, M. Bogus, M. G. Soloway, M. D.
1094 Wilkerson, Y. Cun, J. D. McKay, D. Moro-Sibilot, C. G. Brambilla, S. Lantuejoul, N.
1095 Lemaitre, A. Soltermann, W. Weder, V. Tischler, O. T. Brustugun, M. Lund-Iversen, Å.
1096 Helland, S. Solberg, S. Ansén, G. Wright, B. Solomon, L. Roz, U. Pastorino, I. Petersen, J.
1097 H. Clement, J. Sänger, J. Wolf, M. Vingron, T. Zander, S. Perner, W. D. Travis, S. A. Haas,
1098 M. Olivier, M. Foll, R. Büttner, D. N. Hayes, E. Brambilla, L. Fernandez-Cuesta, R. K.
1099 Thomas, Integrative genomic profiling of large-cell neuroendocrine carcinomas reveals
1100 distinct subtypes of high-grade neuroendocrine lung tumors. *Nat. Commun.* **9**, 1048 (2018).

1101 41. T. Ito, S. Kudoh, T. Ichimura, K. Fujino, W. A. M. A. Hassan, N. Udaka, Small cell lung
1102 cancer, an epithelial to mesenchymal transition (EMT)-like cancer: significance of inactive
1103 Notch signaling and expression of achaete-scute complex homologue 1. *Hum. Cell*. **30**, 1–
1104 10 (2017).

1105 42. A. Augert, E. Eastwood, A. H. Ibrahim, N. Wu, E. Grunblatt, R. Basom, D. Liggitt, K. D.
1106 Eaton, R. Martins, J. T. Poirier, C. M. Rudin, F. Milletti, W.-Y. Cheng, F. Mack, D.
1107 MacPherson, Targeting NOTCH activation in small cell lung cancer through LSD1
1108 inhibition. *Sci. Signal.* **12**, eaau2922 (2019).

1109 43. M. G. Oser, A. H. Sabet, W. Gao, A. A. Chakraborty, A. C. Schinzel, R. B. Jennings, R.
1110 Fonseca, D. M. Bonal, M. A. Booker, A. Flaifel, J. S. Novak, C. L. Christensen, H. Zhang,
1111 Z. T. Herbert, M. Y. Tolstorukov, E. J. Buss, K.-K. Wong, R. T. Bronson, Q.-D. Nguyen, S.
1112 Signoretti, W. G. Kaelin, The KDM5A/RBP2 histone demethylase represses NOTCH
1113 signaling to sustain neuroendocrine differentiation and promote small cell lung cancer
1114 tumorigenesis. *Genes Dev.* **33**, 1718–1738 (2019).

1115 44. P. Baldelli, J. Meldolesi, *eneuro*, in press, doi:10.1523/ENEURO.0010-15.2015.

1116 45. J. Drouin-Ouellet, S. Lau, P. L. Brattås, D. Rylander Ottosson, K. Pircs, D. A. Grassi, L. M.
1117 Collins, R. Vuono, A. Andersson Sjöland, G. Westergren-Thorsson, C. Graff, L. Minthon,
1118 H. Toresson, R. A. Barker, J. Jakobsson, M. Parmar, REST suppression mediates neural
1119 conversion of adult human fibroblasts via microRNA-dependent and -independent
1120 pathways. *EMBO Mol. Med.* **9**, 1117–1131 (2017).

1121 46. J. Charbord, P. Poydenot, C. Bonnefond, M. Feyeux, F. Casagrande, B. Brinon, L.
1122 Francelle, G. Aurégan, M. Guillermier, M. Cailleret, P. Viegas, C. Nicoleau, C. Martinat, E.
1123 Brouillet, E. Cattaneo, M. Peschanski, M. Lechuga, A. L. Perrier, High throughput
1124 screening for inhibitors of REST in neural derivatives of human embryonic stem cells

1125 reveals a chemical compound that promotes expression of neuronal genes: HTS for REST
1126 Inhibitors in Human NSCs. *STEM CELLS.* **31**, 1816–1828 (2013).

1127 47. Y. Ran, F. Hossain, A. Pannuti, C. B. Lessard, G. Z. Ladd, J. I. Jung, L. M. Minter, B. A.
1128 Osborne, L. Miele, T. E. Golde, γ-Secretase inhibitors in cancer clinical trials are
1129 pharmacologically and functionally distinct. *EMBO Mol. Med.* **9**, 950–966 (2017).

1130 48. Y. H. Kim, L. Girard, C. P. Giacomini, P. Wang, T. Hernandez-Boussard, R. Tibshirani, J.
1131 D. Minna, J. R. Pollack, Combined microarray analysis of small cell lung cancer reveals
1132 altered apoptotic balance and distinct expression signatures of MYC family gene
1133 amplification. *Oncogene*. **25**, 130–138 (2006).

1134 49. R. J. Cardnell, L. Li, T. Sen, R. Bara, P. Tong, J. Fujimoto, A. S. Ireland, M. R. Guthrie, S.
1135 Bheddah, U. Banerjee, N. N. Kalu, Y.-H. Fan, S. J. Dylla, F. M. Johnson, I. I. Wistuba, T.
1136 G. Oliver, J. V. Heymach, B. S. Glisson, J. Wang, L. A. Byers, Protein expression of TTF1
1137 and cMYC define distinct molecular subgroups of small cell lung cancer with unique
1138 vulnerabilities to aurora kinase inhibition, DLL3 targeting, and other targeted therapies.
1139 *Oncotarget*. **8**, 73419–73432 (2017).

1140 50. T. K. Owonikoko, S. E. Dahlberg, G. L. Sica, L. I. Wagner, J. L. Wade, G. Srkalovic, B. W.
1141 Lash, J. W. Leach, T. B. Leal, C. Aggarwal, S. S. Ramalingam, Randomized Phase II Trial
1142 of Cisplatin and Etoposide in Combination With Veliparib or Placebo for Extensive-Stage
1143 Small-Cell Lung Cancer: ECOG-ACRIN 2511 Study. *J. Clin. Oncol.* **37**, 222–229 (2019).

1144 51. Y. Liu, H. Yu, S. Yoo, E. Lee, A. Laganà, S. Parekh, E. E. Schadt, L. Wang, J. Zhu, A
1145 Network Analysis of Multiple Myeloma Related Gene Signatures. *Cancers*. **11**, 1452
1146 (2019).

1147 52. J. D. Buenrostro, P. G. Giresi, L. C. Zaba, H. Y. Chang, W. J. Greenleaf, Transposition of
1148 native chromatin for fast and sensitive epigenomic profiling of open chromatin, DNA-
1149 binding proteins and nucleosome position. *Nat. Methods*. **10**, 1213–1218 (2013).

1150 53. F. Ramírez, F. Dündar, S. Diehl, B. A. Grüning, T. Manke, deepTools: a flexible platform
1151 for exploring deep-sequencing data. *Nucleic Acids Res.* **42**, W187-191 (2014).

1152 54. J. T. Robinson, H. Thorvaldsdóttir, W. Winckler, M. Guttman, E. S. Lander, G. Getz, J. P.
1153 Mesirov, Integrative genomics viewer. *Nat. Biotechnol.* **29**, 24–26 (2011).

1154 55. S. Li, C. Wan, R. Zheng, J. Fan, X. Dong, C. A. Meyer, X. S. Liu, Cistrome-GO: a web
1155 server for functional enrichment analysis of transcription factor ChIP-seq peaks. *Nucleic*
1156 *Acids Res.* **47**, W206–W211 (2019).

1157 56. J. G. Doench, N. Fusi, M. Sullender, M. Hegde, E. W. Vaimberg, K. F. Donovan, I. Smith,
1158 Z. Tothova, C. Wilen, R. Orchard, H. W. Virgin, J. Listgarten, D. E. Root, Optimized
1159 sgRNA design to maximize activity and minimize off-target effects of CRISPR-Cas9. *Nat.*
1160 *Biotechnol.* **34**, 184–191 (2016).

1161 57. N. E. Sanjana, O. Shalem, F. Zhang, Improved vectors and genome-wide libraries for
1162 CRISPR screening. *Nat. Methods*. **11**, 783–784 (2014).

1163 58. N. L. Bray, H. Pimentel, P. Melsted, L. Pachter, Near-optimal probabilistic RNA-seq
1164 quantification. *Nat. Biotechnol.* **34**, 525–527 (2016).

1165 59. M. I. Love, W. Huber, S. Anders, Moderated estimation of fold change and dispersion for
1166 RNA-seq data with DESeq2. *Genome Biol.* **15**, 550 (2014).

1167

Figure 1

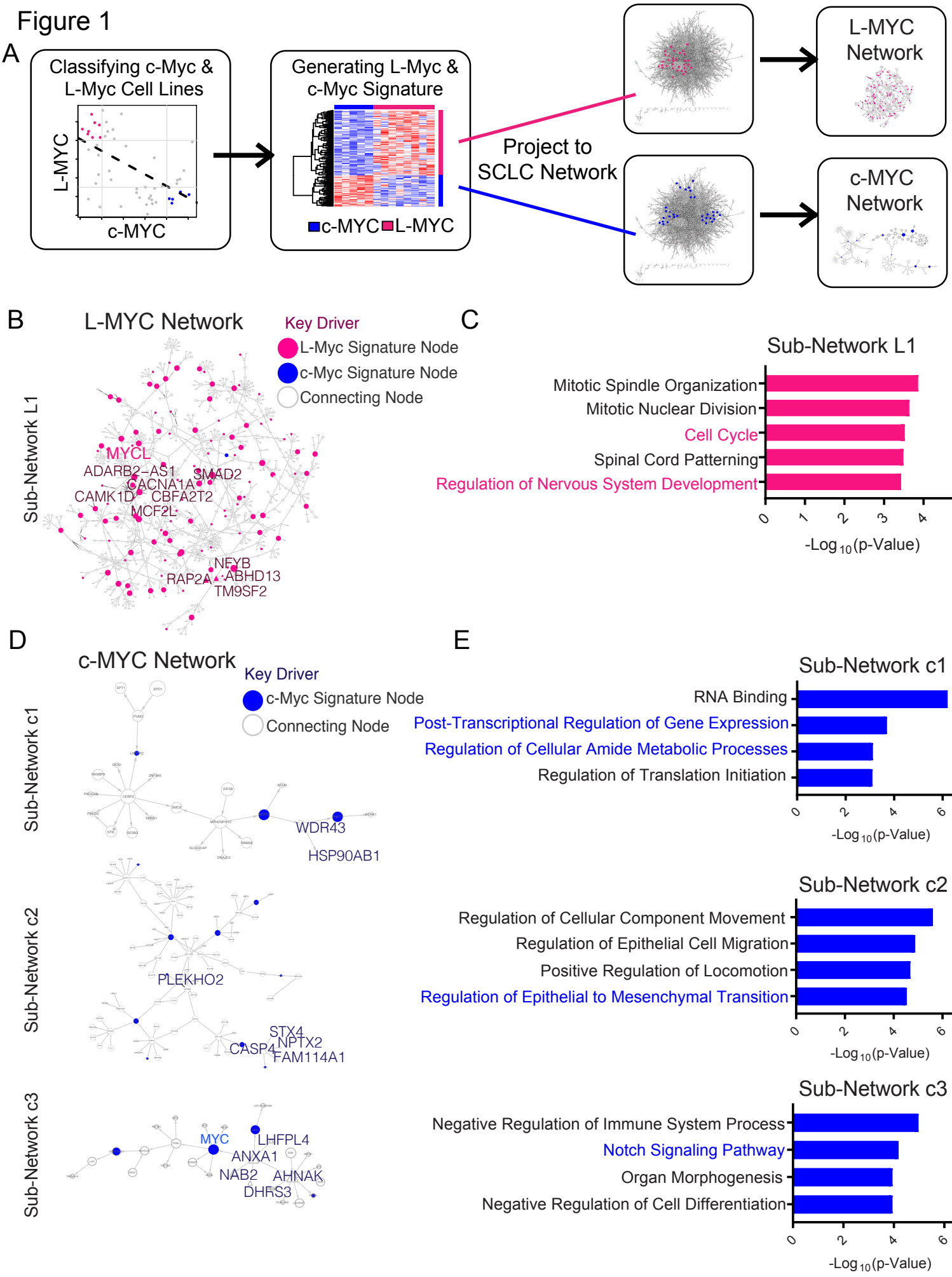
A
Classifying c-Myc & L-Myc Cell Lines
L-MYC
c-MYC
Generating L-Myc & c-Myc Signature
c-MYC L-MYC
Project to SCLC Network
L-MYC Network
c-MYC Network
B
L-MYC Network
Key Driver
L-Myc Signature Node
c-Myc Signature Node
Connecting Node
Sub-Network L1
MYCL
ADARB2-AS1
SMAD2
CACNA1A
CAMK1D
CBFA2T2
MCF2L
NFYB
RAP2A
ABHD13
TM9SF2
C
Sub-Network L1
Mitotic Spindle Organization
Mitotic Nuclear Division
Cell Cycle
Spinal Cord Patterning
Regulation of Nervous System Development
0 1 2 3 4 5
-Log 10(p-Value)
D
c-MYC Network
Key Driver
c-Myc Signature Node
Connecting Node
Sub-Network c1
WDR43
HSP90AB1
Sub-Network c2
PLEKHO2
STX4
NPTX2
CASP4
FAM114A1
Sub-Network c3
MYC
LHFPL4
ANXA1
NAB2
AHNAK
DHRS3
E
Sub-Network c1
RNA Binding
Post-Transcriptional Regulation of Gene Expression
Regulation of Cellular Amide Metabolic Processes
Regulation of Translation Initiation
0 2 4 6
-Log 10(p-Value)
Sub-Network c2
Regulation of Cellular Component Movement
Regulation of Epithelial Cell Migration
Positive Regulation of Locomotion
Regulation of Epithelial to Mesenchymal Transition
0 2 4 6
-Log 10(p-Value)
Sub-Network c3
Negative Regulation of Immune System Process
Notch Signaling Pathway
Organ Morphogenesis
Negative Regulation of Cell Differentiation
0 2 4 6
-Log 10(p-Value)

Figure 2

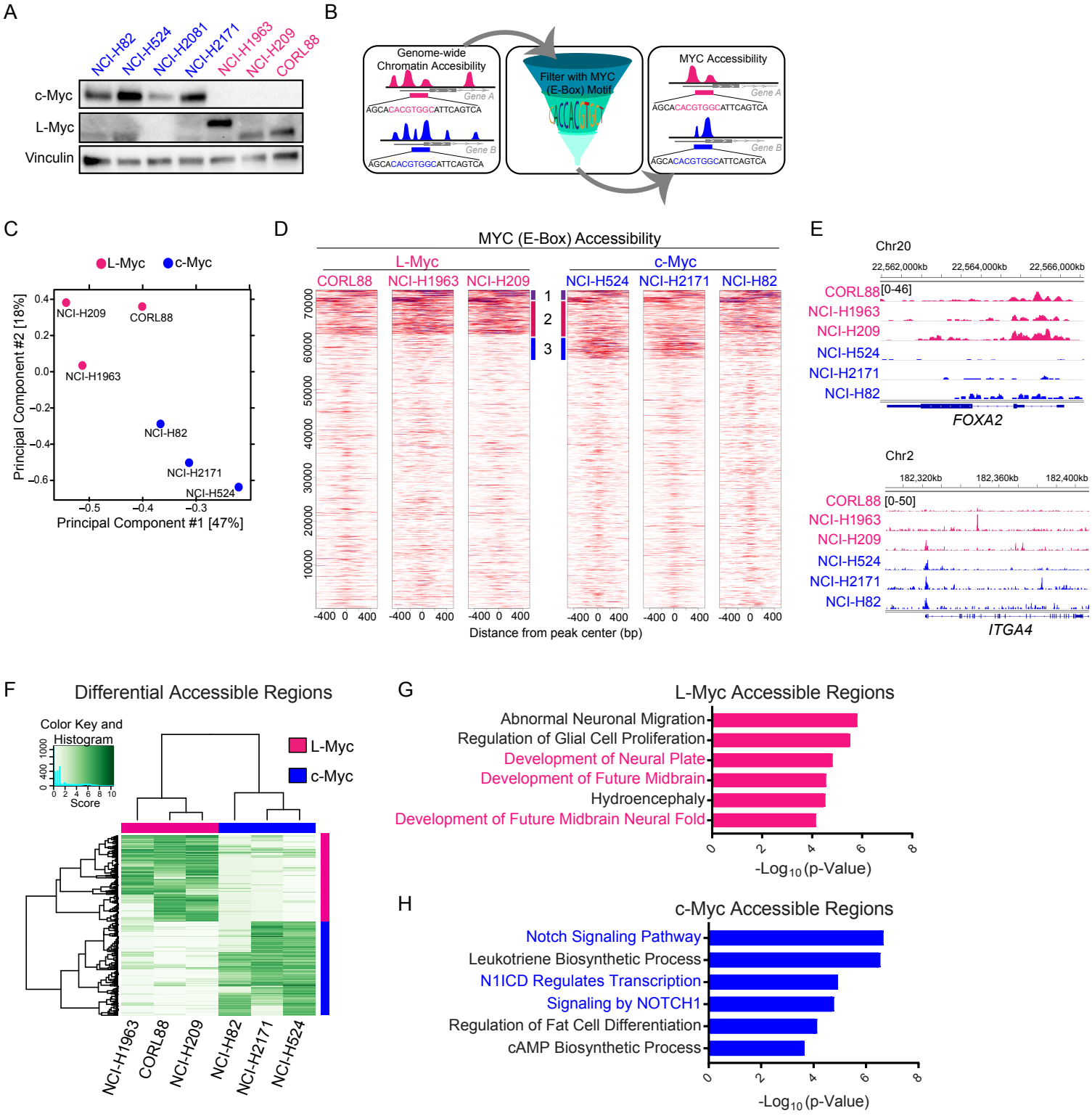
A
NCI-H82
NCI-H524
NCI-H2081
NCI-H2171
NCI-H1963
NCI-H209
CORL88
c-Myc
L-Myc
Vinculin
B
Genome-wide Chromatin Accesibility
Gene A
AGCACACGTGGCATTCAGTCA
Gene B
AGCACACGTGGCATTCAGTCA
Filter with MYC (E-Box) Motif
MYC Accessibility
C
L-Myc
c-Myc
Principal Component #2 [18%]
Principal Component #1 [47%]
NCI-H209
CORL88
NCI-H1963
NCI-H82
NCI-H2171
NCI-H524
D
MYC (E-Box) Accessibility
L-Myc
c-Myc
CORL88
NCI-H1963
NCI-H209
NCI-H524
NCI-H2171
NCI-H82
Distance from peak center (bp)
E
Chr20
22,562,000kb
22,564,000kb
22,566,000kb
[0-46]
FOXA2
Chr2
182,320kb
182,360kb
182,400kb
[0-50]
ITGA4
F
Differential Accessible Regions
Color Key and Histogram
Score
L-Myc
c-Myc
NCI-H1963
CORL88
NCI-H209
NCI-H82
NCI-H2171
NCI-H524
G
L-Myc Accessible Regions
Abnormal Neuronal Migration
Regulation of Glial Cell Proliferation
Development of Neural Plate
Development of Future Midbrain
Hydroencephaly
Development of Future Midbrain Neural Fold
-Log10 (p-Value)
H
c-Myc Accessible Regions
Notch Signaling Pathway
Leukotriene Biosynthetic Process
N1ICD Regulates Transcription
Signaling by NOTCH1
Regulation of Fat Cell Differentiation
cAMP Biosynthetic Process
-Log10 (p-Value)

Figure 3

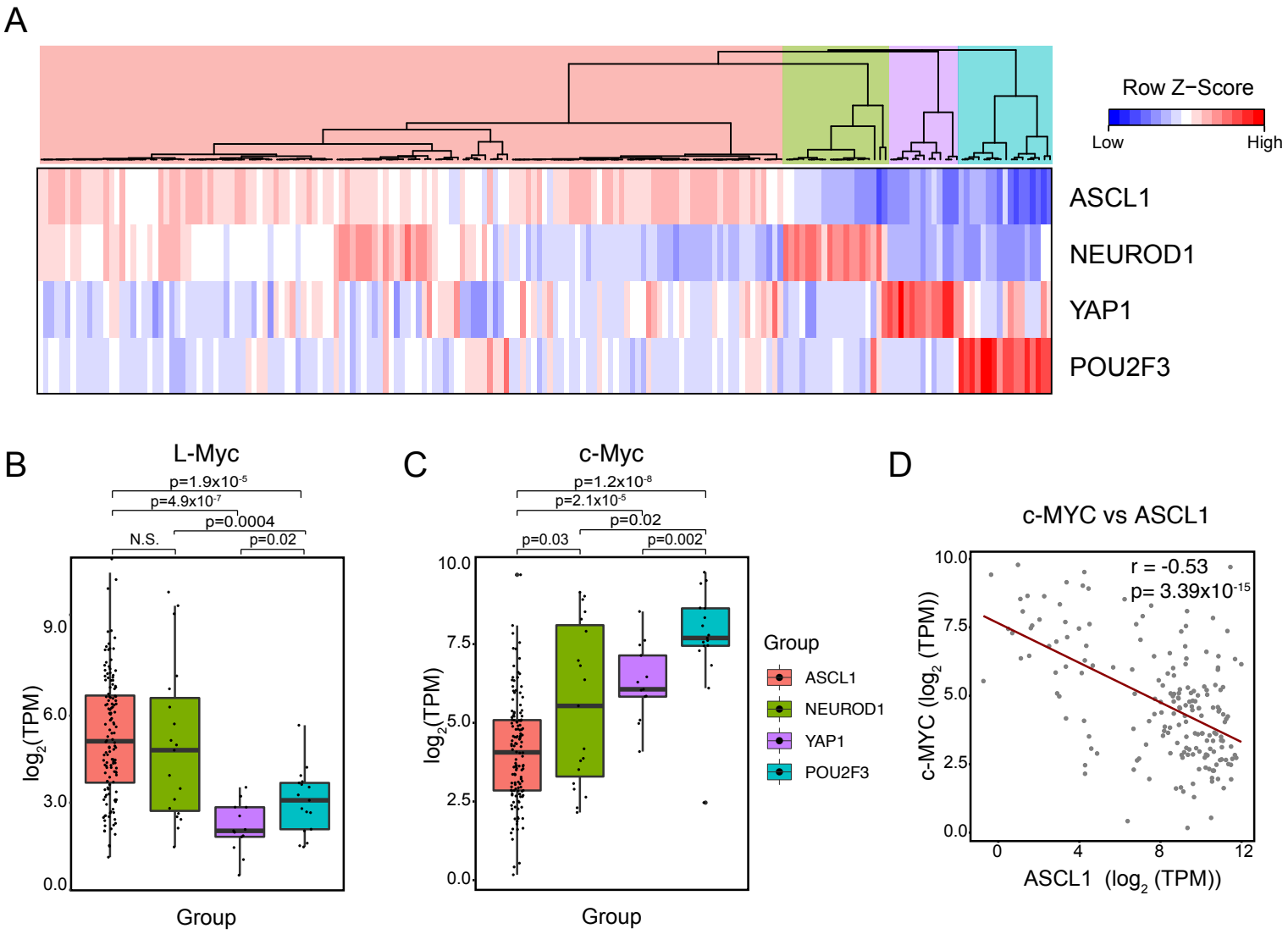
A
Row Z−Score
Low
High
ASCL1
NEUROD1
YAP1
POU2F3
B
L-Myc
p=1.9x10-5
p=4.9x10-7
p=0.0004
N.S.
p=0.02
log2(TPM)
Group
C
c-Myc
p=1.2x10-8
p=2.1x10-5
p=0.02
p=0.03
p=0.002
log2(TPM)
Group
Group
ASCL1
NEUROD1
YAP1
POU2F3
D
c-MYC vs ASCL1
r = -0.53
p= 3.39x10-15
c-MYC (log2 (TPM))
ASCL1 (log2 (TPM))

Figure 4

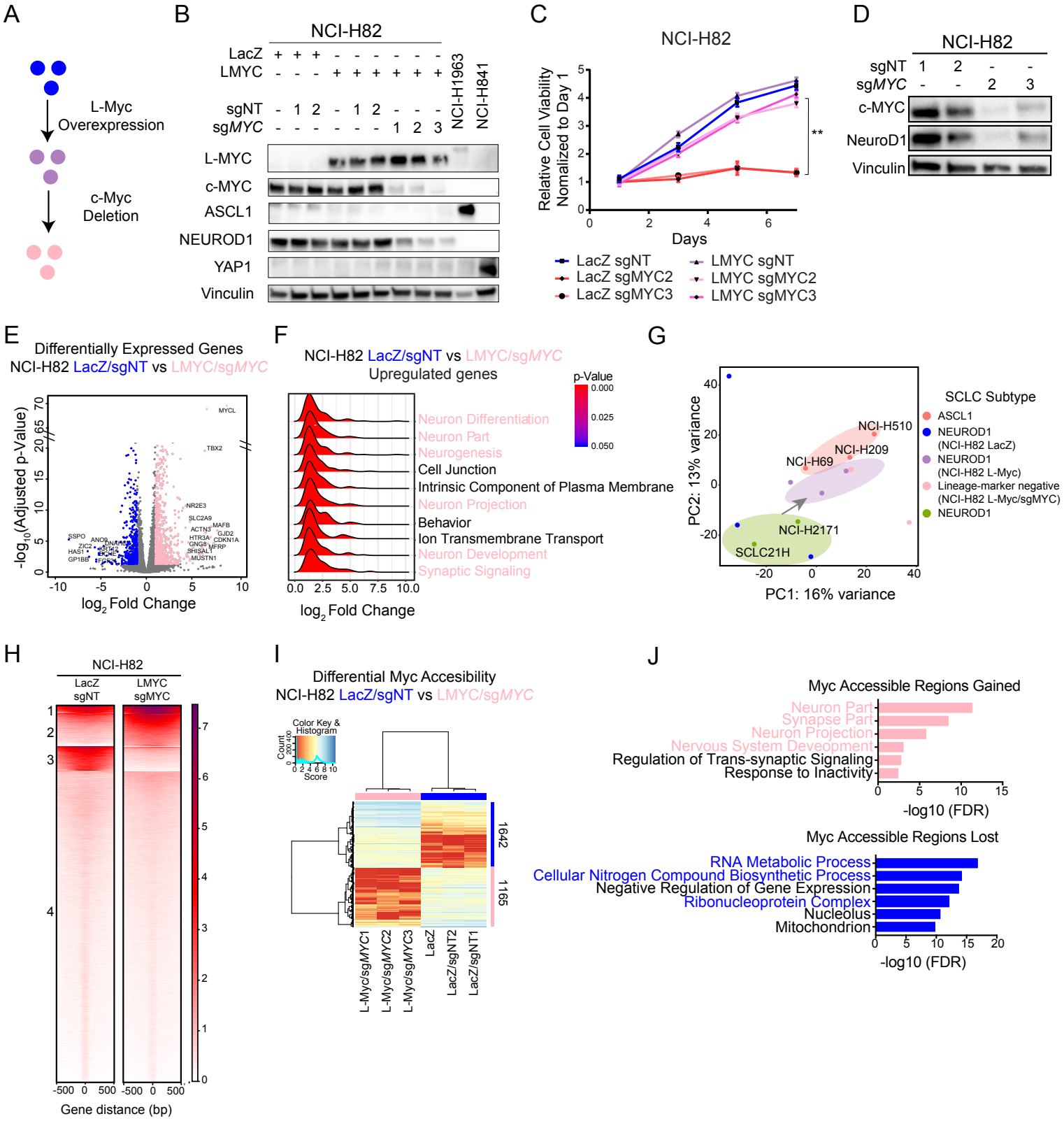

A
L-Myc Overexpression
c-Myc Deletion
B
NCI-H82
LacZ
LMYC
sgNT
sgMYC
NCI-H1963
NCI-H841
L-MYC
c-MYC
ASCL1
NEUROD1
YAP1
Vinculin
C
NCI-H82
Relative Cell Viability Nomalized to Day 1
Days
LacZ sgNT
LacZ sgMYC2
LacZ sgMYC3
LMYC sgNT
LMYC sgMYC2
LMYC sgMYC3
D
NCI-H82
sgNT
sgMYC
c-MYC
NeuroD1
Vinculin
E
Differentially Expressed Genes
NCI-H82 LacZ/sgNT vs LMYC/sgMYC
-log10(Adjusted p-Value)
log2 Fold Change
F
NCI-H82 LacZ/sgNT vs LMYC/sgMYC
Upregulated genes
p-Value
Neuron Differentiation
Neuron Part
Neurogenesis
Cell Junction
Intrinsic Component of Plasma Membrane
Neuron Projection
Behavior
Ion Transmembrane Transport
Neuron Development
Synaptic Signaling
log2 Fold Change
G
SCLC Subtype
ASCL1
NEUROD1 (NCI-H82 LacZ)
NEUROD1 (NCI-H82 L-Myc)
Lineage-marker negative (NCI-H82 L-Myc/sgMYC)
NEUROD1
NCI-H510
NCI-H209
NCI-H69
NCI-H2171
SCLC21H
PC2: 13% variance
PC1: 16% variance
H
NCI-H82
LacZ sgNT
LMYC sgMYC
Gene distance (bp)
I
Differential Myc Accesibility
NCI-H82 LacZ/sgNT vs LMYC/sgMYC
Color Key & Histogram
Count
Score
1642
1165
L-Myc/sgMYC1
L-Myc/sgMYC2
L-Myc/sgMYC3
LacZ
LacZ/sgNT2
LacZ/sgNT1
J
Myc Accessible Regions Gained
Neuron Part
Synapse Part
Neuron Projection
Nervous System Deveopment
Regulation of Trans-synaptic Signaling
Response to Inactivity
-log10 (FDR)
Myc Accessible Regions Lost
RNA Metabolic Process
Cellular Nitrogen Compound Biosynthetic Process
Negative Regulation of Gene Expression
Ribonucleoprotein Complex
Nucleolus
Mitochondrion
-log10 (FDR)

Figure 5

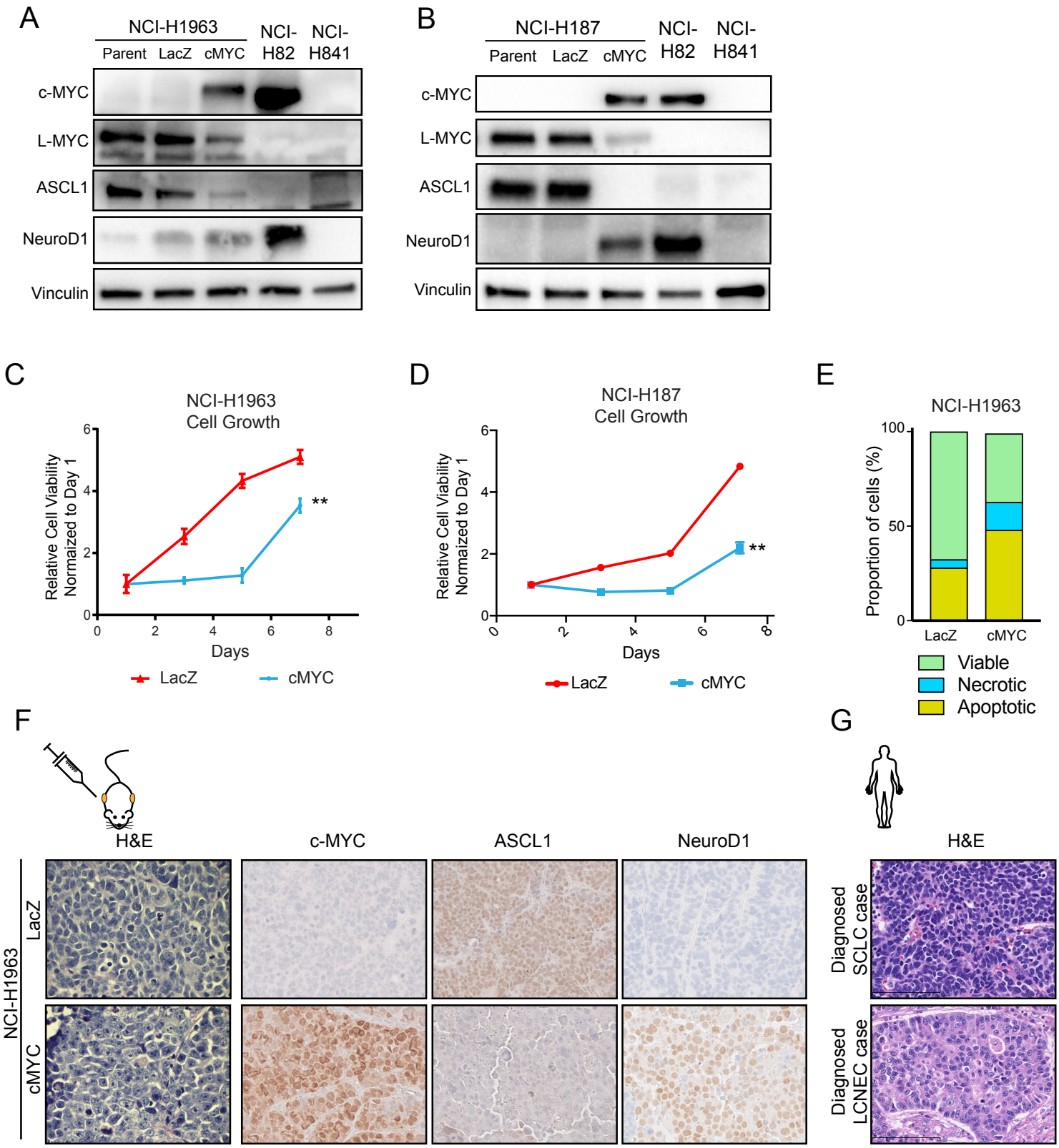
A
NCI-H1963
Parent
LacZ
cMYC
NCI-H82
NCI-H841
c-MYC
L-MYC
ASCL1
NeuroD1
Vinculin
B
NCI-H187
Parent
LacZ
cMYC
NCI-H82
NCI-H841
c-MYC
L-MYC
ASCL1
NeuroD1
Vinculin
C
NCI-H1963
Cell Growth
Relative Cell Viability
Normaized to Day 1
Days
**
LacZ
cMYC
D
NCI-H187
Cell Growth
Relative Cell Viability
Normaized to Day 1
Days
**
LacZ
cMYC
E
NCI-H1963
Proportion of cells (%)
LacZ
cMYC
Viable
Necrotic
Apoptotic
F
H&E
c-MYC
ASCL1
NeuroD1
NCI-H1963
LacZ
cMYC
G
H&E
Diagnosed SCLC case
Diagnosed LCNEC case

Figure 6

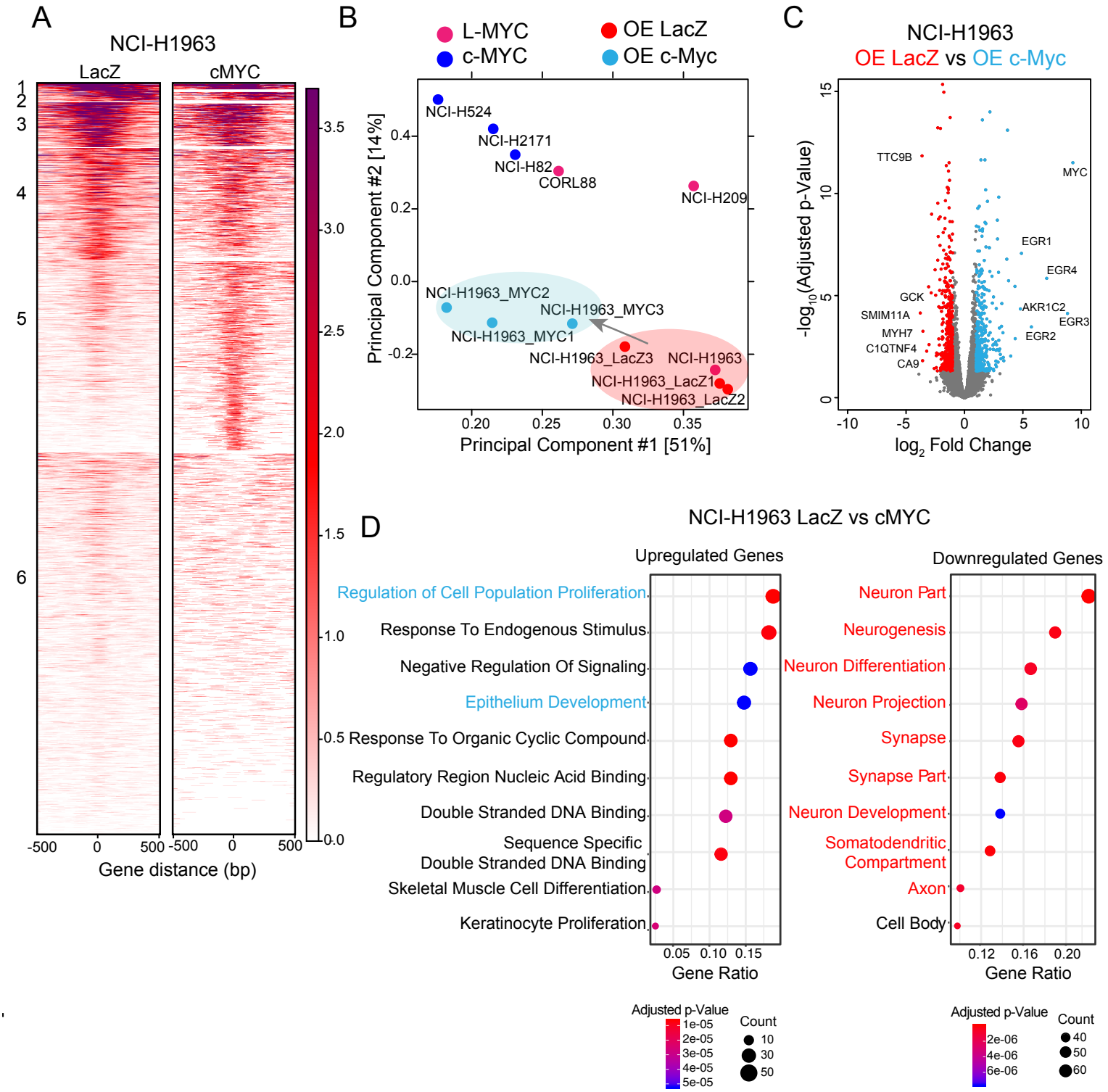
A
NCI-H1963
LacZ
cMYC
1
2
3
4
5
6
-500
0
500
Gene distance (bp)
3.5
3.0
2.5
2.0
1.5
1.0
0.5
0.0
B
L-MYC
c-MYC
OE LacZ
OE c-Myc
NCI-H524
NCI-H2171
NCI-H82
CORL88
NCI-H209
NCI-H1963_MYC2
NCI-H1963_MYC3
NCI-H1963_MYC1
NCI-H1963_LacZ3
NCI-H1963
NCI-H1963_LacZ1
NCI-H1963_LacZ2
Principal Component #2 [14%]
Principal Component #1 [51%]
C
NCI-H1963
OE LacZ vs OE c-Myc
TTC9B
MYC
EGR1
EGR4
GCK
SMIM11A
MYH7
C1QTNF4
CA9
AKR1C2
EGR3
EGR2
-log10(Adjusted p-Value)
log2 Fold Change
D
NCI-H1963 LacZ vs cMYC
Upregulated Genes
Regulation of Cell Population Proliferation
Response To Endogenous Stimulus
Negative Regulation Of Signaling
Epithelium Development
Response To Organic Cyclic Compound
Regulatory Region Nucleic Acid Binding
Double Stranded DNA Binding
Sequence Specific Double Stranded DNA Binding
Skeletal Muscle Cell Differentiation
Keratinocyte Proliferation
Gene Ratio
Adjusted p-Value
1e-05
2e-05
3e-05
4e-05
5e-05
Count
10
30
50
Downregulated Genes
Neuron Part
Neurogenesis
Neuron Differentiation
Neuron Projection
Synapse
Synapse Part
Neuron Development
Somatodendritic Compartment
Axon
Cell Body
Gene Ratio
Adjusted p-Value
2e-06
4e-06
6e-06
Count
40
50
60

Figure 7

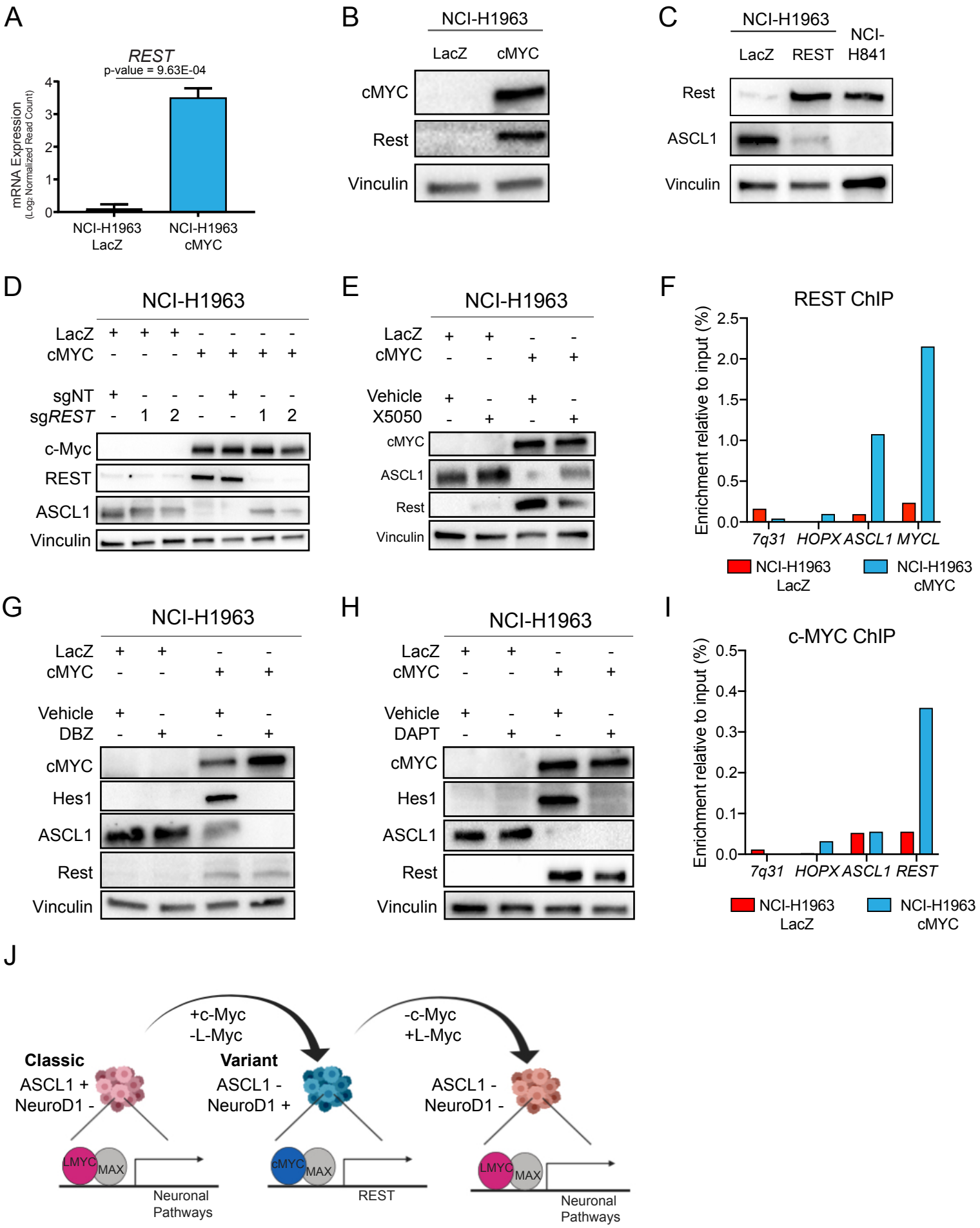
A
REST
p-value = 9.63E-04
mRNA Expression
(Log2 Normalized Read Count)
NCI-H1963 LacZ
NCI-H1963 cMYC
B
NCI-H1963
LacZ
cMYC
cMYC
Rest
Vinculin
C
NCI-H1963
LacZ
REST
NCI-H841
Rest
ASCL1
Vinculin
D
NCI-H1963
LacZ
cMYC
sgNT
sgREST
c-Myc
REST
ASCL1
Vinculin
E
NCI-H1963
LacZ
cMYC
Vehicle
X5050
cMYC
ASCL1
Rest
Vinculin
F
REST ChIP
Enrichment relative to input (%)
7q31
HOPX
ASCL1
MYCL
NCI-H1963 LacZ
NCI-H1963 cMYC
G
NCI-H1963
LacZ
cMYC
Vehicle
DBZ
cMYC
Hes1
ASCL1
Rest
Vinculin
H
NCI-H1963
LacZ
cMYC
Vehicle
DAPT
cMYC
Hes1
ASCL1
Rest
Vinculin
I
c-MYC ChIP
Enrichment relative to input (%)
7q31
HOPX
ASCL1
REST
NCI-H1963 LacZ
NCI-H1963 cMYC
J
+c-Myc
-L-Myc
-c-Myc
+L-Myc
Classic
ASCL1 +
NeuroD1 -
Variant
ASCL1 -
NeuroD1 +
ASCL1 -
NeuroD1 -
LMYC
MAX
cMYC
MAX
LMYC
MAX
Neuronal Pathways
REST
Neuronal Pathways